EXPERIMENTAL INVESTIGATION OF THE INFLUENCE OF VARIOUS NANOPARTICLES ON WATER-BASED MUD

By

Paritosh Dhiman, B.Tech.

A Project Submitted in Partial Fulfillment of the Requirements

for the Degree of

Master of Science

In

Petroleum Engineering

University of Alaska Fairbanks

December 2016

APPROVED:

Dr. Yin Zhang, Committee Chair

Dr. Abhijit Dandekar, Committee Member

Dr. Shirish Patil, Committee Member

Dr. Lei Zhang, Committee Member

Dr. Abhijit Dandekar, Chair

Department of Petroleum Engineering

ABSTRACT

In the oil and gas industry, drilling fluids play an important role in the success of drilling operations. Hence, it is vital to predict accurately and maintain drilling fluid properties. Drilling fluids have multitude of functions, including but not limited to balancing the formation pressure, transporting cuttings, lubricating the bit, minimizing formation damage and maintaining well stability. Efficient completion of any drilling operation is governed by the selection of the proper drilling fluid. Growing hydrocarbon demand is driving the industry to explore unconventional resources such as shale formations and deep water and ultra-deep water areas where high-temperature high pressure (HTHP) conditions persist. Generally, oil-based muds have been widely used in HTHP operations, as they can withstand high temperatures while offering high lubricity, but they are expensive and have an environmental impact. Water-based muds offer a cost-effective and environment-friendly option, but they have limited HTHP application, as they tend to break down, resulting in increased fluid loss and viscosity reduction. Also, upon exposure to high temperatures, they also face the issue of gelation and degradation of weighing materials and additives. Due to these issues with both oil-based muds and water-based muds, new drilling fluids are formulated regularly and the existing systems are tailored to curtail drilling operation costs. Most recently, nanoparticles have been recognized as an effective additive to improve the performance of drilling fluids, having the potential to overcome the limitations of current drilling fluid systems in challenging conditions. In this study, experiments have been conducted to investigate the impact of different nanoparticles on various drilling fluid properties, including rheology, filtration, and lubricity, considering a wide range of influence factors, such as nanoparticle concentration, particle size, nanoparticle type, temperature, and aging. The effect of nanoparticle concentrations (0.01 wt% ~ 1wt%) on drilling fluid properties has been first investigated using SiO_2 nanoparticles with and without coating. Then the effect of nanoparticle size (5 nm ~ 50 nm) on drilling fluid properties has been examined using TiO_2 nanoparticles. Subsequently, the impact of nanoparticle type, including four different nanoparticles, on drilling fluid properties has been tested. Moreover, the effects of temperature and aging on the nanoparticle-based drilling fluid properties have been investigated.

DEDICATION

I dedicate this work to my parents and almighty God.

Table of Contents

Page

List of Figures

Page

List of Tables

Page

ACKNOWLEDGEMENTS

First of all, I would like to extend my gratitude to the chair of my advisory committee, Dr. Yin Zhang, for his invaluable guidance, encouragement and constant support during the entire duration of this project. It gives me great pleasure to show my appreciation to my committee members, Dr. Shirish Patil, Dr. Abhijit Dandekar and Dr. Lei Zhang for their valuable suggestions during this work. I have learned a lot from them.

I wish to thank Dr. Shirish Patil for his time he spent with me as the member for this project. Dr. Patil was able to provide valuable assistance when needed from King Fahd University of Petroleum and Minerals (KFUPM) in Saudi Arabia, where he is now Saudi Aramco Chair Professor of Petroleum Engineering. His assistance and contributions, even though it was 12 hr difference in time zones, are highly appreciated. Also, I would like to thank KFUPM for allowing Dr. Patil to dedicate his time towards this effort while he is working there.

A huge shout out to my parents, who are greater than God for me. Words cannot suffice to describe their unconditional emotional and financial support. I will remain in debt to them forever.

Last but not the least, I would like to thank all my friends during this journey for their words of wisdom and comfort during hours of need.

Chapter 1.

INTRODUCTION

Advancements in drilling and drilling fluid techniques have led to the rapid development of drilling challenging wells, such as ultra-deep wells and high temperature and high pressure (HTHP) wells. Drilling fluids, also known as drilling muds, have many essential functions, such as suspending and carrying cuttings to the surface; controlling formation pressure; stabilizing the wellbore; sealing permeable formations; cooling, lubricating and supporting the drill string and bit; and ensuring drilling efficiency and safety. The cost of drilling fluids can be about 5% to 15% of the total cost of drilling a well, which is expensive (Bloys et al., 1994), though the consequences of not maintaining proper mud properties may result in severe drilling accidents which would require significant time and costs to resolve. Therefore, efforts have been made to improve the properties of the drilling fluids to make the drilling process more efficient, economical, and safe.

Water was used as a drilling fluid as early as the third century BC in China, while mud mixed with water and clay became the definite part of a drilling system in Spindletop Field, Texas, in 1901 (Nasser et al., 2013). In the 20^{th} century, drilling fluid performance was recognized as a primary factor in efficient, economical and safe drilling processes. Therefore, with advancements in drilling technology, more and more additives have been developed and added to the drilling fluids to improve their performance in order to satisfy the requirements of the more advanced drilling techniques. For example, soluble potassium salts along with water-based drilling fluid have been used to mitigate challenges of wellbore instability associated with drilling in shales (Mondshine, 1973). In addition, issues related to HTHP wells have been proven to be harder to mitigate, while drilling fluids such as lignite/polymer mud have been developed to handle these issues (Mitchell et al., 1990). Furthermore, challenges met in drilling depleted reservoirs and underpressure zones have promoted the development of wellbore strengthening techniques. Accordingly, Gilsonite or cellulose fibers, which act as bridging agents, have been developed and applied in the drilling of depleted reservoirs to seal micro-fractures and reduce transmission of pore pressure (Newhouse, 1991).

Entering the 21st century, depletion of conventional oil and gas reserves and increasing energy demand have attracted much more attention to drilling more challenging wells, such as shale/tight formation drilling, ultra-deep drilling, and HTHP drilling. However, the conventional drilling fluid systems have met their limitations in drilling these challenging wells. For example, regular water-based muds (WBM) can cause significant swelling in shale formations, which would result in severe wellbore instability (Van Oort, 2003). Although KCl-based WBM can inhibit shale swelling and improve well stability effectively, they may cause severe environmental impacts, so their applications have been limited significantly. In addition, WBMs are known to deteriorate when exposed to HTHP conditions commonly associated with deep well drilling and extended reach drilling operations (Abdo and Haneef, 2013). Besides, ultra-deep wells associated with HTHP have been facing the challenges of narrow operating windows, which cause changes in rheology and lead to ECD control issues resulting in potential lost circulation (Ravi, 2011). The non-aqueous muds, such as oil-based muds (OBM), are more lubricious, less corrosive, better at shale swelling inhibition, and better able to withstand lower and higher temperatures as compared to WBM (Growcock and Patel, 2011). However, the OBMs have distinct disadvantages, such as environmental impacts, high costs, and safety and health issues (Patel et al., 2007), limiting their wide applications in some particular areas, such as offshore and Arctic drilling (Neff, 2010). Therefore, more efficient and cost-effective drilling fluid systems are required for drilling these challenging wells successfully.

In the last two decades, nanoparticles have been applied widely in various fields, such as medicine, electronics, food processing, and materials manufacturing, due to their unique physicochemical, thermal, electrical, hydrodynamic and interaction properties (Ravichandran, 2010). Most recently, nanoparticles have been recognized as an effective additive to improve the performance of drilling fluids, having the potential to overcome the limitations of current drilling fluid systems that are met in drilling more challenging wells (Al-Yasiri and Al-Sallami, 2015). Cai et al. (2011) tested the influence of seven different non-modified commercially available silica nanoparticles with sizes between 7 nm to 20 nm on the performance of bentonite drilling fluid. They found that the nanoparticles reduced the permeability of the Atoka shale by 99.3% at 10 wt% concentration. Thus, the water invasion can be reduced significantly, and the shale swelling can be inhibited, which has been commonly recognized (Sensoy et al., 2009; Sharma et al., 2012; Pham and Nguyen, 2014; Moslemizadeh and Shadizadeh, 2015). However, the conclusions about the influence of

nanoparticles on API standard filtration are inconsistent (Zakaria et al., 2012; Fakoya and Shah, 2014; Kang et al., 2016; Salih et al., 2016). For example, Vryzas et al. (2015) tested the effect of iron oxide and silica nanoparticles on the performance of bentonite-based drilling fluids. They found that iron oxide nanoparticles can enhance filtration properties at an optimal concentration of 0.5 wt%, whereas silica nanoparticles adversely affected fluid loss characteristics. Also, they found that both nanoparticles can modify the muds' rheological properties, which has been widely recognized (Jung et al., 2011; Sharma et al., 2012; Nasser et al., 2013; Fakoya and Shah, 2013). Until now, limited studies have been conducted to investigate the influence of nanoparticles on mud lubricity, and their findings are not consistent (Abdo and Haneef, 2013; Nasser et al., 2013; Wrobel, 2016). Besides, although extensive studies have been carried out on nanoparticle-based muds, each single study is not very comprehensive: the influence of only a few nanoparticles on specific mud function has been tested and limited influence factors, such as only temperature and/or concentration, have been investigated. This is why some findings about the influence of nanoparticles on some mud properties, such as filtration and lubricity, are not consistent.

In this study, experiments have been conducted to investigate the impact of different nanoparticles on various drilling fluid properties including rheology, filtration, and lubricity, while a wide range of influence factors, such as nanoparticle concentration, nanoparticle size, nanoparticle types, temperature, and aging, have been considered. The effect of nanoparticle concentrations (0.01 wt% ~ 1wt%) on drilling fluid properties was first investigated using SiO_2 nanoparticles with and without coating, and then the effect of nanoparticle size (5 nm ~ 50 nm) on drilling fluid properties was examined using TiO_2 nanoparticles. Subsequently, the impact of nanoparticle type, including four different nanoparticles, on drilling fluid properties was tested. Moreover, the effect of temperature and aging on the nanoparticle-based drilling fluid properties has been investigated.

Chapter 2.

LITERATURE REVIEW

The selection of the proper drilling fluid for the required job is an integral part of the drilling process. The drilling fluid selection process comprise of selecting an appropriate type of drilling fluid and deciding its composition in accordance with the kind of formation and conditions in which it will be used. Broadly, drilling fluids are classified on the basis of their base fluids. They classified into three major types: liquids, gases and gas-liquid mixtures, and selected on the basis of their need and functionality. Fig. 1 represents a hierarchal classification of drilling fluids.

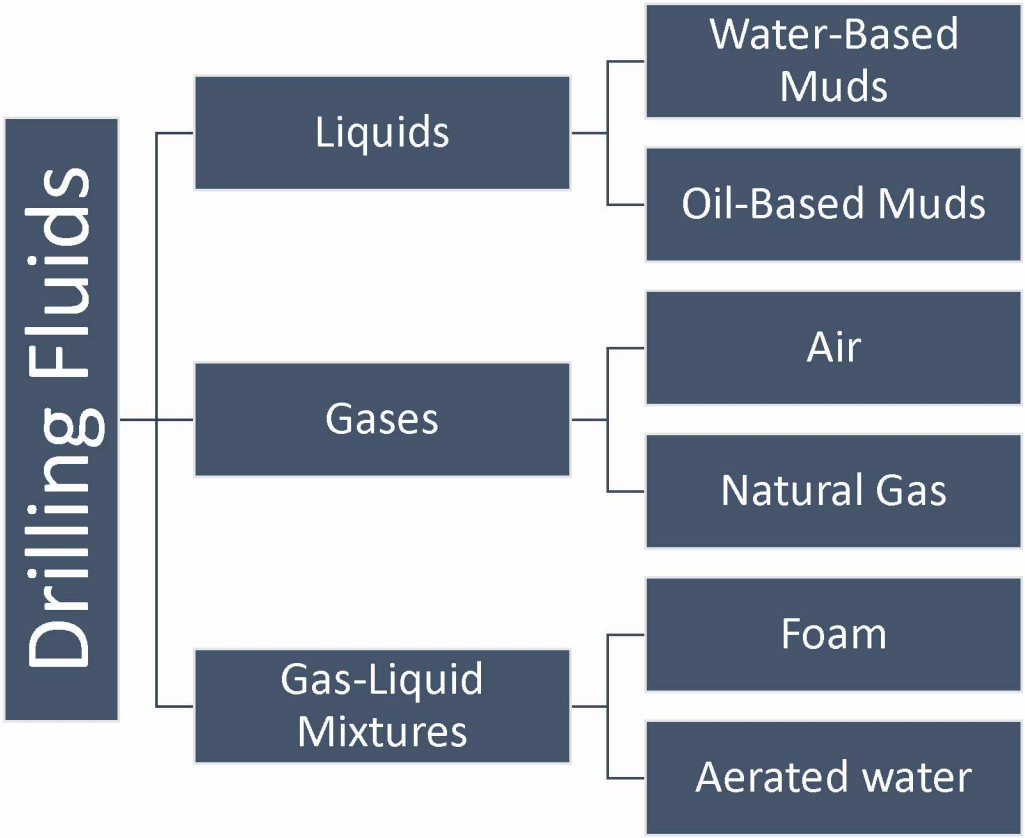

Figure 1: Drilling Fluids Classification

2.1 Types of Drilling Fluids

2.1.1 Water-Based Muds (WBM)

As the name suggests, this mud type uses water or brine as its base fluid. They are also referred as aqueous drilling fluids. Due to their environment-friendly nature, easy disposal and cost efficient operation, they are used widely in the industry. Based on the type of additives used to enhance their properties, they are further classified into salt water muds, dispersed muds, non-dispersed muds, low solids muds, polymer muds and calcium muds. They have a tendency to cause well stability issues by causing swelling in shales. Also, they provide limited lubrication to drill bits, which restricts their use in extended reach drilling.

2.1.2 Oil-Based Muds (OBM)

These type of drilling muds have oil in the continuous phase, which could be mineral oil, diesel oil or low-toxicity linear olefins and paraffins. Compared to WBM, their formulation is complex and expensive. They are known to provide sufficient lubrication to drill bits, restrict shale swelling, provide excellent cutting carrying and have good filtration control. Even though they have the edge over WBMs, their use is limited due to environmental and disposal issues. Depending on the type of continuous phase, they are further classified into invert emulsion muds and emulsion muds. They are classified as invert emulsion muds if they have water in oil emulsions, with a continuous phase comprising diesel or mineral oil. Emulsion muds have oil dispersed in water, with water as the continuous phase.

2.1.3 Gas Drilling Muds

Gas drilling muds find their application in underbalanced drilling where the pressure in the wellbore is kept lower than the fluid pressure in the formation being drilled (https://petrowiki.org/PEH%3AUnderbalanced_Drilling). They provide the advantage of no solid contamination, as there are no solids and contact involved. Their other benefits include no lost circulation, no formation damage and high rate of penetration. Depending upon the type of gas used, they are classified into air and natural gas drilling muds.

2.1.4 Foam Drilling Muds

Foam drilling muds find their application in underbalanced, deep water and ultra-deep water drilling. They are mostly used in places which have narrow operating pressure windows, which means that a slight decrease in mud density would allow the formation fluids to influx into the wellbore and a slight increase in mud density would be enough to initiate micro or macro fractures in the formation. Usually, foam drilling muds comprise 75-95% gaseous phase, 5-25% liquid phase and about 5% surfactant, which is used as a stabilizer (Shah et al., 2010). The gaseous phase is usually an inert gas such as nitrogen, and the liquid phase can be either brine or fresh water. Foam drilling muds are also classified as stable foam drilling muds and stiff foam drilling muds.

2.2 Functions of Drilling Fluids

Drilling fluids have various functions, most of which are essential to every well. Additives can be introduced into the drilling fluids to enhance their properties, in order to achieve certain functions specific to the well requirements. The primary purpose of drilling fluids in every well is to control formation pressures and remove cuttings from the well (MISWACO, 1998).

Although the importance of drilling fluid functionality is governed by well operation and condition, the most common functions of drilling fluids are:

1. Control formation pressures.
2. Suspend cuttings when circulation stops.
3. Transport cuttings from the well.
4. Help in sealing permeable formations.
5. Maintain wellbore stability.
6. Minimize formation damage.
7. Help in formation evaluation.
8. Lubricate, cool and support the bit and drilling assembly.
9. Transmit hydraulic energy to downhole equipment.
10. Aid in corrosion control.
11. Minimize environmental impacts.

Even though all the functions of drilling fluids are necessary, sometimes, in order to adapt and perform efficiently in a particular formation, the drilling fluid may not be able to perform all the functions. Thus, the best compromise is balancing all the needs and functions of the drilling fluid. During drilling fluid design, preference is given to the most essential functions and the mud is designed in accordance with the requirements of the operation.

2.3 Rheology

Rheology is defined as the study of deformation and flow of matter (MISWACO, 1998). Rheology is one of the most important properties of drilling fluids; it provides information about how the fluid would behave under different conditions and what its viscosity profile would be under different shear rates. Information about the viscosity profile aids in predicting friction pressure losses and better design of the drilling fluid, and thus better performance. Fluid behavior is determined by the relationship between shear stress and shear rate. According to the shear stress vs. shear rate relationship, the fluid can be described by a number of fluid models. If this relationship is linear, then the fluid can be termed a Newtonian fluid. Otherwise, if the relationship is non-linear, then it is known as a non-Newtonian fluid. In the oil and gas industry, most drilling fluids are non-Newtonian fluids described by non-Newtonian fluid models such as the Bingham plastic model, the Power-law model, or the Herschel-Bulkley model (MISWACO, 1998).

Mathematically, shear rate for a fluid flowing between two parallel plates is represented by:

$$\gamma = \frac{dv}{dy} \qquad \text{eq.1}$$

where v is the velocity of the moving plate and y is the distance between the two parallel plates.

Shear stress is given by:

$$\sigma = \frac{F}{A} \qquad \text{eq.2}$$

where F is the shear force and A is the area acted on by the shear force.

For a Newtonian fluid, shear stress and shear rate have a linear relationship, which is represented by a straight line on a Cartesian plot passing through the origin, described by the equation:

$$\sigma = \mu * \gamma \qquad \text{eq.3}$$

where σ is the shear stress, μ is the viscosity and γ is the shear rate.

As stated before, non-Newtonian fluids do not have a linear relationship between shear stress and shear rate. One of the simplest models to describe non-Newtonian fluids is the Bingham plastic model. The Bingham plastic model is also termed as a two-point model as it needs two points, the yield point and plastic viscosity, to describe fluid behavior. It also represents a linear relationship between shear stress and shear rate, but the straight line does not intercept the origin. The model equation is similar to the Newtonian fluid equation with the addition of the yield point. The Bingham plastic model is represented by the equation:

$$\sigma = \sigma_y + \mu_p * \gamma \qquad \text{eq.4}$$

where μ_p is the plastic viscosity and σ_y is the yield point.

Another common model used to represent non-Newtonian fluids is the Power-law model. The fluids described by this model are often termed shear thinning fluids or pseudoplastic fluids. The equation that describes the Power-law model is:

$$\sigma = K * \gamma^n \qquad \text{eq.5}$$

where K *i*s the consistency index and n is the power law index.

For this model, viscosity is defined by:

$$\mu_a = K * \gamma^{n-1} \qquad \text{eq.6}$$

where μ_a is the apparent viscosity, which decreases as the shear rate increases. Due to this behavior, the fluids described by this model are termed shear thinning fluids.

2.4 Lubricity

Lubricity comes into consideration when two bodies are in contact; the contact can be rolling, sliding or separating in nature. When two bodies are in contact, they produce frictional force at their interface in the direction opposite to their movement. This force of friction is known to cause wear, thus damaging one or both bodies at the contacting surfaces. In order to lower the amount of friction and wear, lubricants are used, and the process is termed lubrication (Jones, 1971).

2.5 Filtration

When the mud has higher pressure than the formation pressure, the mud filtrate is forced to go into the formation. While doing so, it deposits solids on the borehole wall, leaving behind a mud cake with filtrate invasion. The initial fluid that flows into the formation, before the deposited solids form the mud cake, is known as spurt loss. Both mud cake deposition and filtrate invasion can lead to errors and problems, which may result in significant downtime during the operation. Filtrate invasion causes formation damage and results in a reduction of formation permeability, which subsequently hampers production. The most common experiment to test the filtration characteristics of the drilling fluid is the API static filtration test, which is a low-pressure low-temperature (LPLT) test.

2.6 Previous Related Work

Nanoparticles have been recognized recently as useful additives to improve drilling fluid performance. They have the potential to overcome the limitations of current drilling fluid systems that are faced while drilling more challenging wells. Until now, mixed success has been attained in research related to nanoparticle application in drilling fluids. The desire to solve existing problems in drilling fluids has inspired researchers to use nanoparticles to enhance wellbore stability, lubricity, filtration and rheological properties.

Sensoy et al. (2009) used two different types of silica nanoparticles, each 20 nm in size, in various concentrations of 40, 29, 10 and 5 wt%, to minimize water invasion. They formed nanoparticle suspensions with mud and tested the ability of the nanoparticle-based muds to plug shale pores. Through their experiments, they found that decreasing nanoparticle concentration to 5 wt% resulted in a higher leak-off into the shale. They also concluded that 10 wt% concentration was ideal for plugging the shale pores. Building on this work, Cai et al. (2011) investigated the effect of different sizes of silica nanoparticles (5 to 20 nm), at 10 wt% concentration, on water invasion into shale. They used two types of base muds, bentonite and low-solids mud, to form nanoparticle-based muds. They observed that nanoparticle sizes between 7 and 15 nm at 10 wt% concentration were effective at reducing shale permeability and thus shale swelling. They also noted that nanoparticle-based muds resulted in higher plastic viscosity and lower yield point and fluid loss compared to the base muds. Knowing that silica nanoparticles can be used to reduce shale swelling,

it was necessary to understand their impact on clay swelling. Pham and Nguyen (2014) studied the effect of silica nanoparticles on clay swelling. They observed that presence of polyethylene glycol (PEG) coated silica nanoparticles had a positive impact on clay swelling inhibition only in the presence of electrolytes. They also concluded that increasing nanoparticle concentration in clay dispersion leads to particle aggregation.

Through the work of Cai et al. (2011), it was evident that nanoparticles can be used to alter rheology and filtration loss characteristics of drilling fluids. Jung et al. (2011) synthesized two different clay nanoparticle hybrids, aluminum oxide-silica nanoparticle clay hybrid (ASCH) and iron oxide nanoparticle clay hybrid (ICH), and tested their effects on the rheological properties of bentonite drilling mud. They found that at 0.5 wt%, ICH was able to increase the viscosity and yield point compared to base mud, which was due to the development of cross-links between the particles. Also, they observed that ASCH association with clay platelets in bentonite drilling fluid is pH sensitive. At high pH, the addition of ASCH resulted in a reduction of viscosity and yield point, however, as pH decreased, its properties became similar to those of ICH. Nasser et al. (2013) used a mixture of nano graphite and nano silicon wires, at 3 wt%, to investigate the effect of prepared nanoparticle-based mud on rheological properties at various temperatures. They found that temperature had a detrimental effect on the rheological properties, and nanoparticle-based mud showed improved lubricity and filtration characteristics.

Zakaria et al. (2012) used in-house prepared nanoparticles to test the filtration characteristics of an oil based mud. They investigated the filtration loss characteristics on API standard filter press (LPLT) and reported a 70% reduction in fluid loss. As stated earlier, Nasser et al. (2013) observed that a mixture of nano graphite and nano silicon wires, at 3 wt%, was able to improve the filtration characteristics of the mud. Vryzas et al. (2015) tested the effect of iron oxide and silica nanoparticles on the performance of bentonite-based drilling fluids. They found that iron oxide nanoparticles can be used to enhance filtration properties at an optimal concentration of 0.5 wt%, whereas silica nanoparticles adversely affected fluid loss characteristics.

Until now, limited studies have been conducted to investigate the influence of nanoparticles on mud lubricity. Abdo and Haneef (2013) tested palygorskite (Pal), a naturally available clay, synthesized into nano-form with an average diameter of 10-20 nm. Drilling fluid samples were formed with 5.9 g of Pal in the presence of 40 g montmorillonite with 570 ml of water. This

drilling fluid recipe was found to improve the lubricity by 33.8%. Wrobel (2016) used different nanoparticles, such as MoS_2, TiO_2 and TiN, in bentonite drilling fluid and investigated their lubricity characteristics. The nanoparticles were added between 0.02 to 0.08 wt% in concentration. MoS_2 was found to improve the lubricity of the mud, with 0.04 wt% being optimal nanoparticle concentration. However, TiO_2 enhanced the lubricity at the lowest concentration of 0.02 wt%; further increases in concentration negatively impacted the lubricity characteristic of the mud. It was also noted that TiN proved to be a bad lubricity agent.

Chapter 3.

EXPERIMENTAL METHOD

3.1 Materials and Equipment

In this study, the base mud is mixed with 5 wt% of bentonite and deionized water. Eight different nanoparticles have been used to prepare nanoparticle-based drilling fluid samples, respectively. Table 1 shows the eight nanoparticles and their corresponding fundamental basic properties.

The CPX Series Ultrasonic Bath, as shown in Fig. 1 (a), has been used to pre-disperse the nanoparticles in deionized water, and then the Qsonica Q500 Sonicator, as shown in Fig. 1 (b), has been used to sonicate the prepared nanoparticle dispersions to disperse the nanoparticles completely. The Hamilton Beach mixer, shown in Fig. 1 (c), has been employed to mix the bentonite and the aqueous phase. The OFITE Model 900 Viscometer associated with a computer control system, shown in Fig. 2 (a), has been used to measure the rheological properties of the drilling fluids. The OFITE API standard LPLT filter press, shown in Fig. 2 (b), has been used to measure the filtration properties of the drilling fluids. The OFITE EP and Lubricity Tester, shown in Fig. 2 (c), has been used to determine the coefficient of lubricity of different drilling fluid samples, and the OFITE Portable Roller Oven and Aging Cells, shown in Fig. 2 (d), have been employed to conduct the aging tests.

Table 1 – Nanoparticles used in this study

Nanoparticle	Size, nm	Bulk Density, g/cm^3	SSA, m^2/g	Electrical Charge	Nature
SiO_2 with KH550 coating	20-30	< 0.1	130-600	Negative	Super oleophilic and hydrophilic, and easier to be dispersed
SiO_2 without coating	20-30	< 0.1	180-600	Negative	Hydrophilic and easier to disperse in ethanol
TiO_2 - Anatase	5	0.12-0.18	289	Positive	Hydrophilic and high catalytic activity
TiO_2 - Anatase	10	0.15-0.25	210	Positive	Hydrophilic and photocatalyst
TiO_2 - Anatase	15	0.22	60	Positive	Hydrophilic and photocatalyst
TiO_2 - Anatase	50	0.42-0.50	20-40	Positive	Hydrophilic and photocatalyst
Al_2O_3	20	0.18-0.30	230-400	Positive	Hydrophilic and high catalytic activity
Fe_3O_4	20	0.85	40-60	Positive	Hydrophilic and super paramagnetic

(a) CPX Series Ultrasonic Bath

(b) Qsonica Q500 Sonicator

(c) Hamilton Beach Mixer

Figure 2 - Drilling Fluid Preparation Equipment

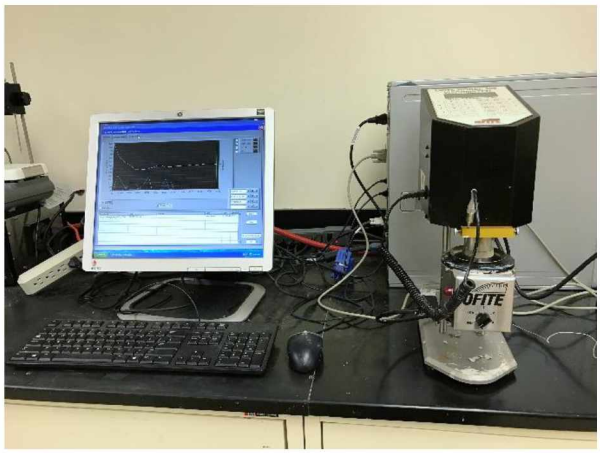

(a) OFITE Model 900 Viscometer

(b) OFITE LPLT Filter Press

(c) OFITE EP and Lubricity Tester

(d) OFITE Portable Roller Oven and Aging Cells

Figure 3 - Laboratory Equipment

3.2 Test Scenarios and Procedures

In this study, four common scenarios have been designed and carried out to investigate the influence of nanoparticles on the properties of drilling fluids including rheology, filtration, and lubricity. Scenario 1 is to test the effect of concentration of two nanoparticles, SiO_2 with KH550 coating and SiO_2 without coating, on the mud properties. Scenario 2 is to examine the effect of the nanoparticle size at a fixed concentration of 0.5 wt% on the mud properties. Scenario 3 is to test the influence of nanoparticle type on mud properties. Scenario 4 is to examine the effect of aging on the properties of the nanoparticle-based muds. In addition, the effect of temperature on the rheological properties of the nanoparticle-based muds, i.e., Scenario 5 in rheology measurement, has been investigated. The details of these test scenarios are described in Table 2.

Table 2 - Test Scenarios

Mud Properties	Test Scenarios	Nanoparticle Type	Nanoparticle Concentration, wt%	Temperature, °C
Rheology	Scenario 1: Effect of Concentration	SiO_2 with KH550 coating	0.01, 0.05, 0.1, 0.25, 0.5, 1	25
		SiO_2 without coating		
	Scenario 2: Effect of Particle Size	TiO_2, 5 nm	0.5	25
		TiO_2, 10 nm	0.5	25
		TiO_2, 15 nm	0.5	25
		TiO_2, 50 nm	0.5	25
	Scenario 3: Effect of Nanoparticle Type	SiO_2 with KH550 coating	0.5	25
		SiO_2 without coating	0.5	25
		Al_2O_3	0.5	25
		Fe_3O_4	0.5	25
	Scenario 4: Effect of Aging	SiO_2 with KH550 coating	0.5	25
		SiO_2 without coating	0.5	25

		TiO_2, 5 nm	0.5	25
		TiO_2, 10 nm	0.5	25
		TiO_2, 15 nm	0.5	25
		TiO_2, 50 nm	0.5	25
		Al_2O_3	0.5	25
		Fe_3O_4	0.5	25
	Scenario 5：Effect of Temperature	SiO_2 with KH550 coating	0.5	25, 40, 60, 80
		SiO_2 without coating		
Filtration	Scenario 1：Effect of Concentration	SiO_2 with KH550 coating	0.01, 0.05, 0.1, 0.25, 0.5, 1	25
		SiO_2 without coating		
	Scenario 2: Effect of Particle Size	TiO_2, 5 nm	0.5	25
		TiO_2, 10 nm	0.5	25
		TiO_2, 15 nm	0.5	25
		TiO_2, 50 nm	0.5	25
	Scenario 3: Effect of Nanoparticle Type	SiO_2 with KH550 coating	0.5	25
		SiO_2 without coating	0.5	25
		Al_2O_3	0.5	25
		Fe_3O_4	0.5	25
	Scenario 4: Effect of Aging	SiO_2 with KH550 coating	0.5	25
		SiO_2 without coating	0.5	25
		TiO_2, 5 nm	0.5	25
		TiO_2, 10 nm	0.5	25
		TiO_2, 15 nm	0.5	25
		TiO_2, 50 nm	0.5	25
		Al_2O_3	0.5	25
		Fe_3O_4	0.5	25

Lubricity	Scenario 1: Effect of Concentration	SiO_2 with KH550 coating	0.01, 0.05, 0.1, 0.25, 0.5, 1	25
		SiO_2 without coating		
	Scenario 2: Effect of Particle Size	TiO_2, 5 nm	0.5	25
		TiO_2, 10 nm	0.5	25
		TiO_2, 15 nm	0.5	25
		TiO_2, 50 nm	0.5	25
	Scenario 3: Effect of Nanoparticle Type	SiO_2 with KH550 coating	0.5	25
		SiO_2 without coating	0.5	25
		Al_2O_3	0.5	25
		Fe_3O_4	0.5	25
	Scenario 4: Effect of Aging	SiO_2 with KH550 coating	0.5	25
		SiO_2 without coating	0.5	25
		TiO_2, 5 nm	0.5	25
		TiO_2, 10 nm	0.5	25
		TiO_2, 15 nm	0.5	25
		TiO_2, 50 nm	0.5	25
		Al_2O_3	0.5	25
		Fe_3O_4	0.5	25

The test procedures are described briefly in the following section.

3.2.1 Drilling Fluid Preparation

The base mud has been prepared by adding bentonite to the deionized water little by little while stirring, and then continuing to stir the mixture for 15 minutes. There are two main steps to prepare the nanoparticle-based muds. The first step is to prepare the nanoparticle dispersions: the nanoparticles are pre-dispersed for 4 hours in the CPX Series Ultrasonic Bath, and then continue to be dispersed for 20 mins using the high-frequency Q500 Sonicator to make sure that the nanoparticles have been dispersed thoroughly. The second step is to add the weighed bentonite

(5wt%) into the prepared nanoparticle dispersions while stirring, and then continuing to stir the mixture for 15 minutes. Then the prepared muds are ready for measurement.

3.2.2 Rheology Measurements

The OFITE Model 900 Viscometer, which is associated with a computer control system and a heating cup, has been used to measure the rheological properties of the prepared base mud and nanoparticle-based muds. The heating cup is used to heat the mud to the test temperature at which the rheological properties need to be measured, while the computer control system is used to set, control and monitor the mud temperature. Also, the computer control system is used to calculate and record the rheology parameters including plastic viscosity (PV), yield point (YP), power law exponent (n), fluid consistency factor (K), and gel strengths.

The detailed measurement procedure is as follows (OFITE Model 900 Viscometer Manual, 2015):

1. Before the test, select and design the type of test to be conducted on the computer control software (ORCADA).
2. Specify the test temperature in ORCADA.
3. Install bob on the bob shaft with the help of shaft wrench.
4. Place the rotor sleeve over the bob and move it upward to connect the rotor.
5. Pour approximately 170 ml of the test fluid into the cup. Then set the cup in the heating container.
6. Raise the sample cup, with the rotor sleeve immersed into the test fluid up to the scribed line.
7. The test is started from ORCADA.

3.2.3 Filtration Measurements

The OFITE LPLT filter press has been employed to measure the filtration properties of prepared base mud and nanoparticle-based muds following the API standard procedures (Reference, API standard). In this study, only 30 minute filtration volume and filter cake thickness have been reported and discussed.

The detailed test procedure is as follows (OFITE API Filter Press Manual, 2013):

1. Before the test, it is vital to make sure that each part of the cell is dry and clean. The gaskets need to be examined for wear and distortion.
2. To assemble the test cell, turn the base cap upside down and place a rubber gasket into it. Then, set a screen along with a filter paper and another gasket on top of it. Lastly, put the cell body into the base cap and lock it.
3. Pour the sample to be tested into the cell, with 0.5 inches of empty space at the top.
4. Place a dry, clean graduated cylinder under the filtrate tube.
5. Make sure that all the valves above the test cells are closed.
6. Apply the pressure of 100 ± 5 psi to the inlet port on the pressure manifold. Open the valve for the cell to be tested. Begin the test period at the time of initial pressurization.
7. Measure the volume of filtrate collected at 1, 7.5, 15 and 30 minutes in ml.
8. After 30 minutes, pull the pressure valve out to release the pressure from the cell. Remove the cell and disassemble it.
9. Carefully remove filter paper with the deposited mud cake.
10. Measure and record the thickness of the filter cake to the nearest $\frac{1}{32}$ inches.

3.2.4 Lubricity Measurements

The OFITE EP and Lubricity Tester has been used to measure the coefficient of lubricity for the prepared base mud and nanoparticle-based muds, while the standard lubricity coefficient test is conducted at a fixed rotation rate of 60 RPM and a fixed force between two hardened steel surfaces of 150 in-lb. Before each mud test, the equipment has been calibrated by determining the correction factor using deionized water, and the correction factor can be calculated as

$$\text{Correction Factor} = \frac{\text{Standard Meter Reading for Deionized Water}}{\text{Meter Reading Obtained in Deionized Water Calibration}} \quad \text{eq.7}$$

Then, the calibrated equipment is used for the mud test, while the lubricity coefficient can be determined by

$$\text{Lubricity Coefficient} = \frac{\text{Meter Reading} * \text{Correction Factor}}{100} \quad \text{eq.8}$$

The detailed operation procedure is as follows (OFITE EP and Lubricity Tester Manual, 2015):

1. Before the test, clean the lubricity test ring and the test block with acetone and rinse both thoroughly with deionized water.
2. Turn on the power and let the machine run for 15 minutes.
3. Position the test block in the block holder, with the concave side of test block facing away from the torque shaft. It is vital for the test ring and block not to be in contact with each other.
4. Set the motor speed to 60 RPM.
5. After the unit has completed running for 15 minutes, zero the torque reading. The unit is run for 5 more minutes and the torque is zeroed again.
6. Fill the test cup with the test sample. Raise the cup stand until the test ring and the black are fully immersed. Zero the torque reading again if necessary.
7. Place the torque arm so that it fits inside the concave portion of the torque arm clamp.
8. Torque handle is turned clockwise until the torque gauge on the arm reads 150 in-lb.
9. The machine is run for 5 minutes and then the torque reading is recorded.
10. The motor speed is adjusted to zero and the cup is lowered.

3.2.5 Aging Test

The prepared muds have been aged by API Recommended Practice 13B-1 and 13I using the OFITE aging cells and OFITE portable roller oven (API RP 13B-1 and 13I). Dynamic aging is carried out at 275^{o}F for 16 hours. Then, the rheological, filtration and lubricity characteristics of the aged muds have been measured following the above measurement procedures and compared with those of the corresponding un-aged muds.

The detailed operation procedure of the aging cell and portable roller oven is as follows (OFITE Portable Roller Oven Manual, 2015):

1. Pour the test sample into the aging cell. Leave approximately 1 inch of empty space at the top. Next, the aging cell is closed.
2. Turn on the portable roller oven.
3. Enter the temperature required for the aging test into the machine along with the duration of aging.
4. Put the aging cell on the rollers.
5. For dynamic aging, place the roller power switch in the "On" position.
6. On completion of aging test, allow the aging cell to cool down to room temperature.
7. After cooling down, extract the sample from the aging cell and stir it in the mechanical mixer for 15 minutes to homogenize the sample.

Chapter 4.

RESULTS AND DISCUSSION

4.1 The Influence on Rheology

In this subsection, the influence of nanoparticle concentration, nanoparticle size, nanoparticle type, aging, and temperature on rheological properties of the nanoparticle-based muds have been investigated, while experimental results have been reported, analyzed and discussed. Also, the rheological values of plastic viscosity, yield point and YP/PV ratio have been compared to the API specifications. Furthermore, their corresponding influence on mud functions has been discussed.

4.1.1 Effect of Concentration

In this scenario, the influence of nanoparticle concentration on the rheological properties of nanoparticle-based muds has been investigated. Both of the nanoparticles used in this scenario are SiO_2. Just one SiO_2 nanoparticle is without any coating, which is hydrophilic, while another SiO_2 nanoparticle is coated with KH550, making it super oleophilic and hydrophilic and easier to disperse. Both the nanoparticles have been tested at concentrations of 0.01, 0.05, 0.1, 0.25, 0.5 and 1 wt%, the results of which are in Fig. 4.

Measurements for SiO_2 with KH550 nanoparticle were within an average relative standard deviation of 2.8% for plastic viscosity (PV), 6.3% for yield point (YP), 4.3% for gel strength (10 min), 4% for power law index (n), 8.4% for consistency index (K) and 5.3% for YP/PV ratio, with 0.5 wt% concentration having the highest relative standard deviation. Which might be due to variation in nanoparticle concentration, because of the use of a weighing balance with one decimal place precision. While, SiO_2 without coating nanoparticle measurements were within 1.4% for PV, 13.6% for YP, 10% for gel strength, 9.2% for power law index, 8.7% for consistency index and 3.7% for YP/PV ratio, with 0.5 wt% again showing the highest relative standard deviation. Which again might be related to the precision of the weighing balance used.

As can be seen from Fig. 4 (a), the plastic viscosity (PV) increases with the nanoparticle concentration due to the fact that the solid content of the drilling fluids continues to increase with the increase of the nanoparticle concentration. The PV increase rate of the mud composed of SiO_2

nanoparticle without coating is higher than that of the mud consisting of SiO_2 nanoparticle coated with KH550, since SiO_2 nanoparticle coated with KH550 has higher density compared to SiO_2 nanoparticle without coating, so the former will have fewer particles in dispersion compared to latter. Mostly, the PV values for both nanoparticle-based muds satisfy the API minmum value, except for 0.01 wt% concentration of SiO_2 with KH550 nanoparticle. As shown in Figs. 4 (b), (c) and (d), the yield points (YP) and gel strengths of both muds decrease with increasing nanoparticle concentration and their downtrends are quite similar. Besides, at lower concentrations (< 0.1 wt%), the YP and gel strength of the nanoparticle-based muds are higher than those of the base mud. However, at higher concentrations (> 0.1 wt%), the YP and gel strength of the nanoparticle-based muds are lower than those of the base mud. All of these phenomena may be explained by the electrical properties of the clay and nanoparticles. In general, the surface of the SiO_2 nanoparticle is negatively charged (Kim et al., 2014), while after dispersion, the surface of the SiO_2 nanoparticle coated with KH550 is also negatively charged due to the hydrolysis reaction of the silane coupling agent. Therefore, both nanoparticles are negatively charged in the dispersions. By introducing a small amount of nanoparticles into the mud, flocculation may occur, resulting in higher YP and gel strength than those of the base mud at the lower nanoparticle concentration. Subsequently, by introducing more negatively charged nanoparticles into the mud, the attractive force between the particles in the mud decreases, which results in the decrease of YP and gel strength with increasing nanoparticle concentration. Also, as can be observed in Fig. 4 (b), the YP values for nanoparticle-based muds are less than that of the specified API maximum value. Hence, they satisfy the API YP requirement.

The influence of nanoparticle concentration on YP/PV ratio; n, which is the power law index; and K, which is the consistency index of the Power-law model, have been described in Figs. 4 (e), (f), and (g), respectively. As can be seen, with increasing nanoparticle concentration, YP/PV ratios decrease, *n* values increase, and K values decrease for both nanoparticles. It is well known that the hole cleaning capacity of the mud can be improved by increasing the YP/PV ratio, lowering the n value, and increasing the K value (Okrajni and Azar, 1986; Bloodworth et al., 1992). Therefore, in this scenario, the hole cleaning capacity of the nanoparticle-based mud decreases with increasing negatively charged SiO_2 nanoparticle concentration. Besides, it can be seen from Figs. 4 (e), (f) and (g) that the YP/PV ratio and K values of the nanoparticle-based muds are higher than those of the base mud at lower concentration (< 0.1 wt%). The n values of the nanoparticle-based

muds are lower than those of the base mud at lower concentrations (< 0.1 wt%). All of these findings indicate that, compared with the base mud, adding a small number of negatively charged SiO_2 nanoparticles (< 0.1 wt%) can improve the mud's hole cleaning capacity, while higher negatively charged SiO_2 nanoparticle concentration (> 0.1 wt%) has an adverse effect. Also, it can be observed from Fig. 4 (e), YP/PV ratio values for nanoparticle-based muds are less than the API maximum value, indicating that the muds satisfy the API requirement.

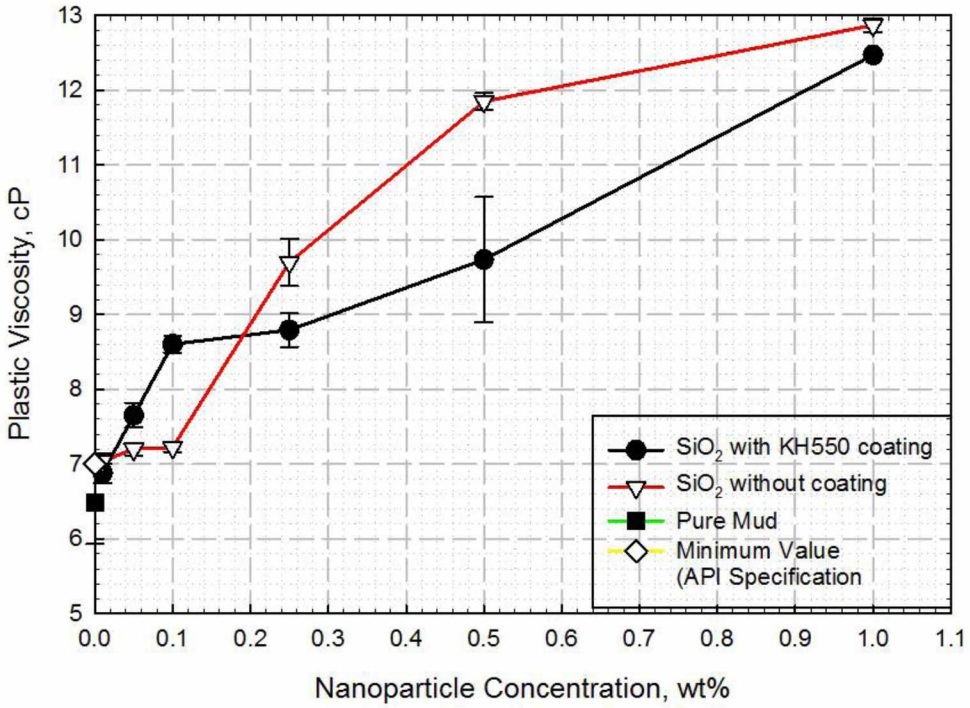

Figure 4 (a): Effect of Nanoparticle Concentration on Plastic Viscosity

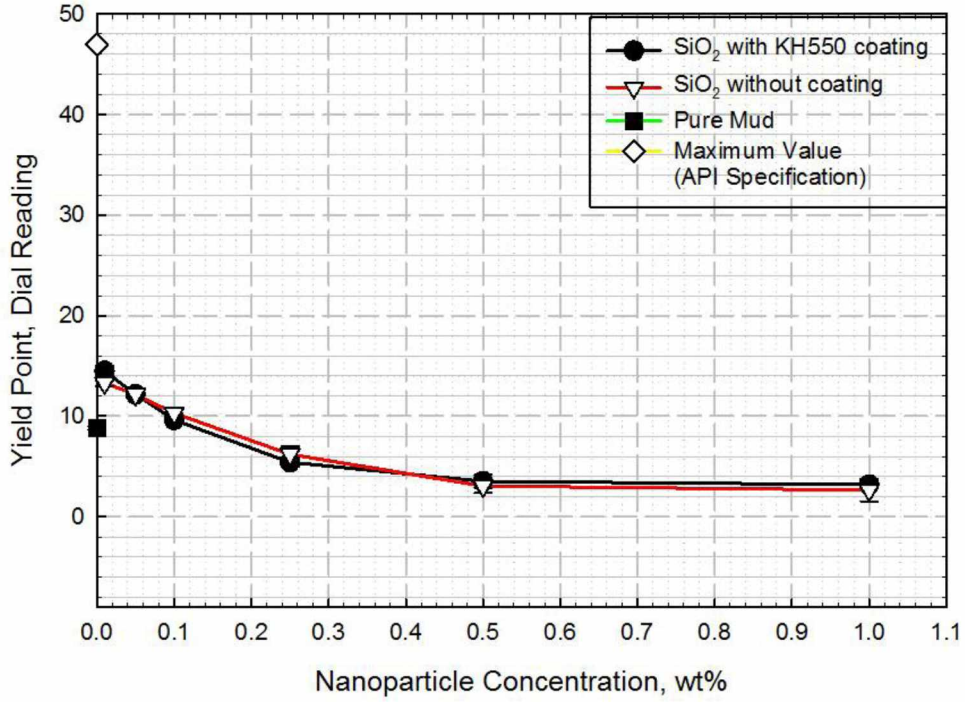

Figure 4 (b): Effect of Nanoparticle Concentration on Yield Point

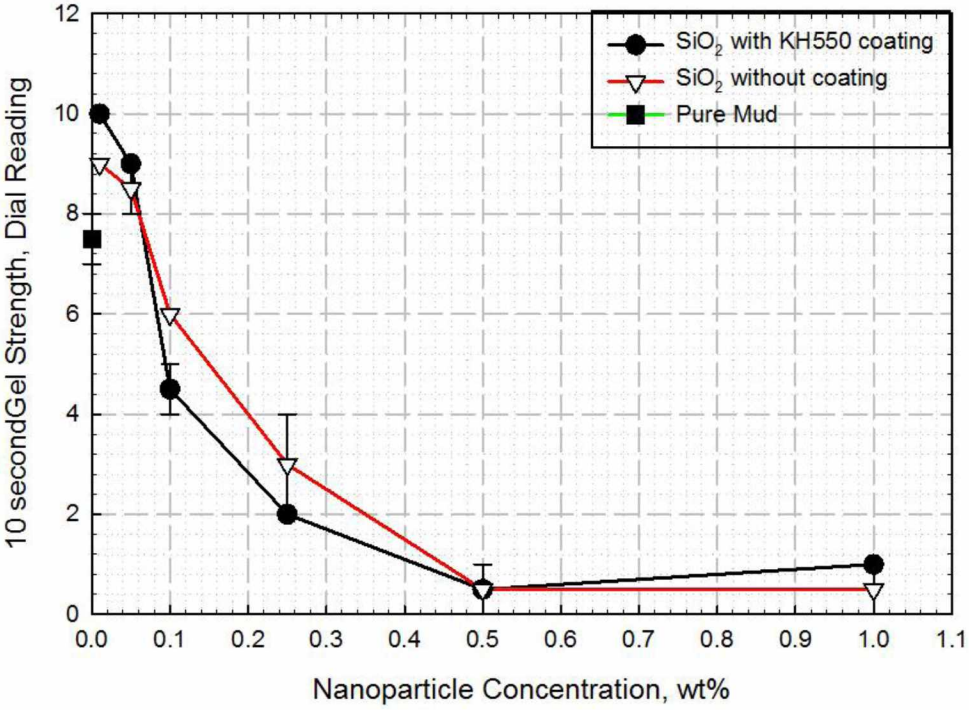

Figure 4 (c): Effect of Nanoparticle Concentration on 10 sec Gel Strength

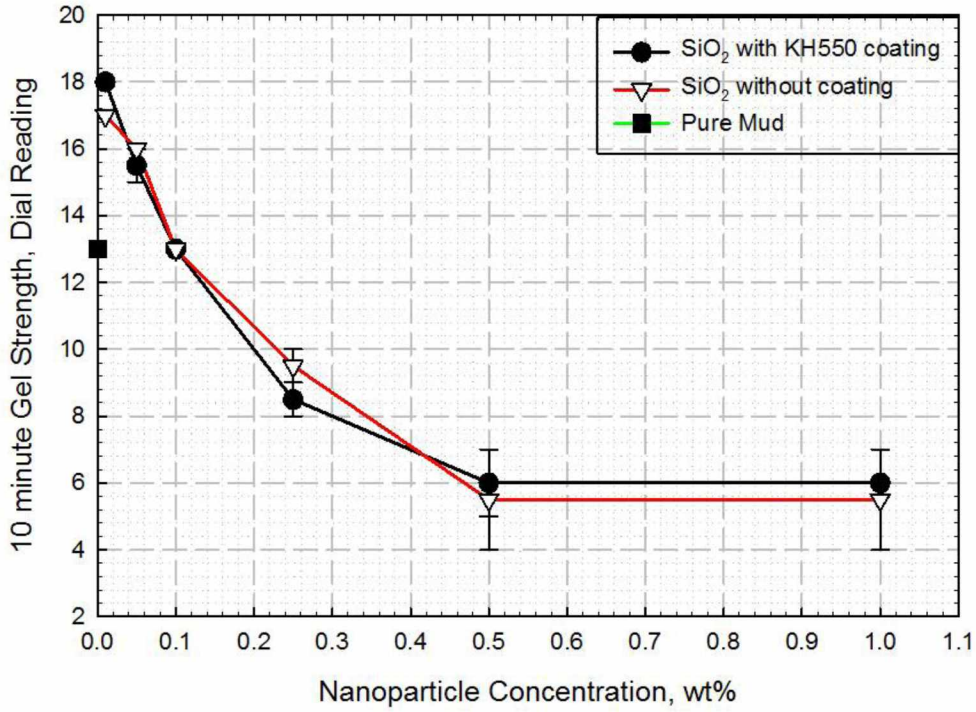

Figure 4 (d): Effect of Nanoparticle Concentration on 10 min Gel Strength

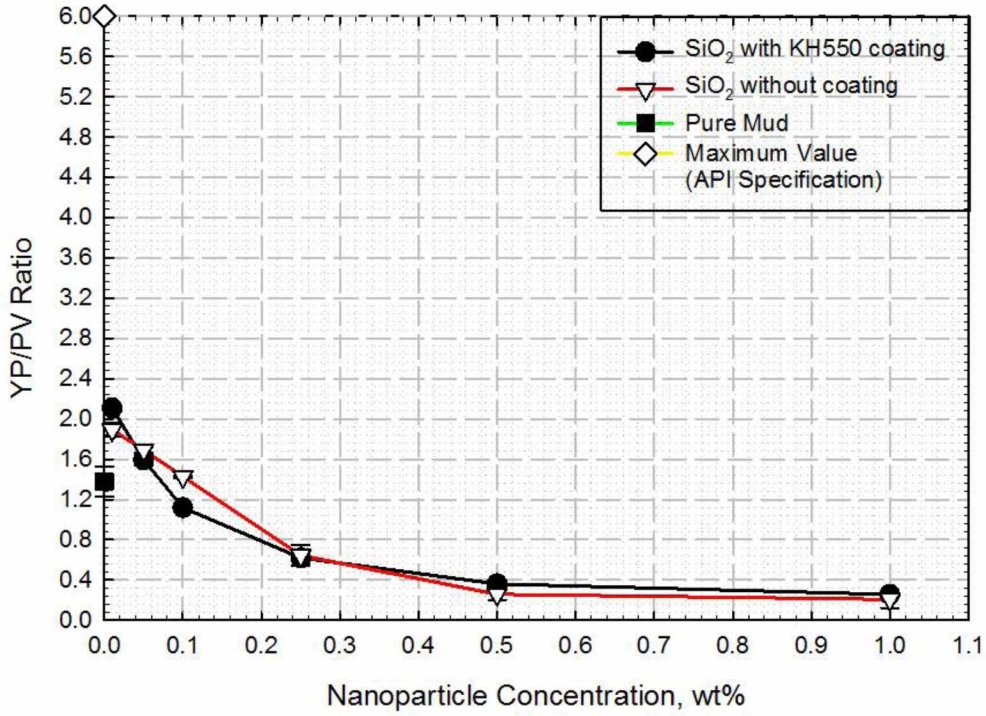

Figure 4 (e): Effect of Nanoparticle Concentration on YP/PV ratio

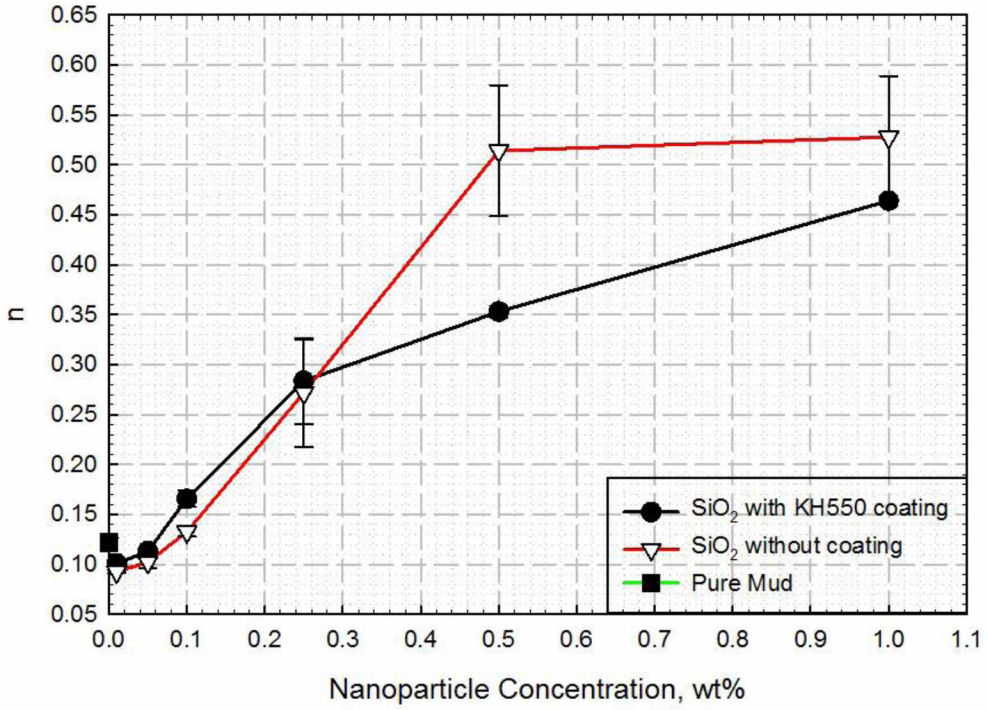

Figure 4 (f): Effect of Nanoparticle Concentration on Power Law Index

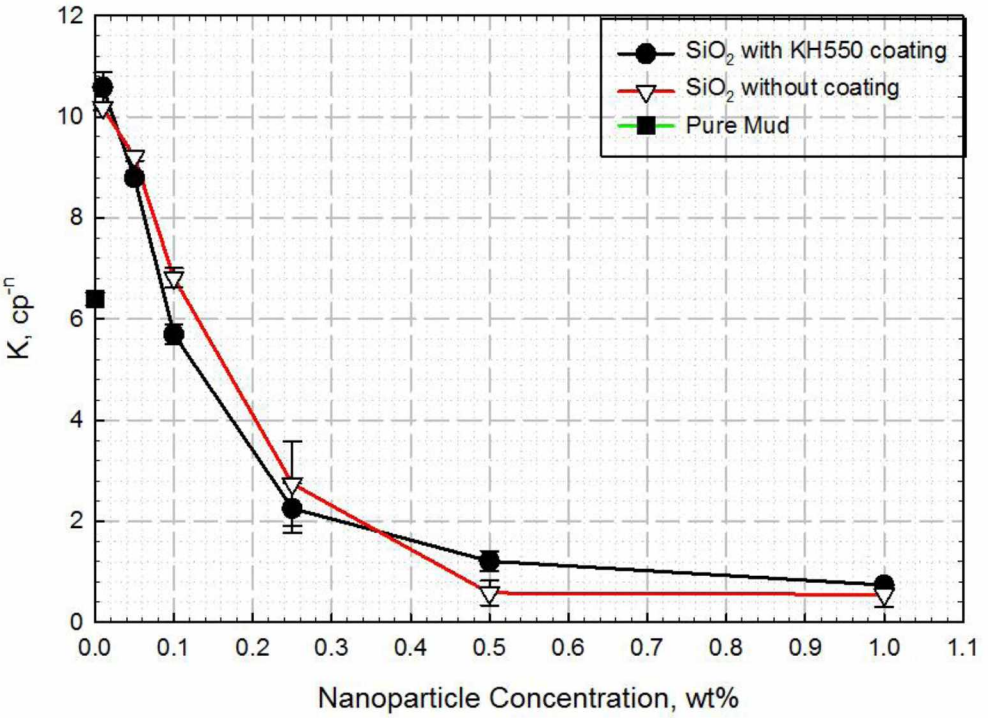

Figure 4 (g): Effect of Nanoparticle Concentration on Consistency Factor

4.1.2 Effect of Size

In this scenario, the influence of nanoparticle size on the rheological properties of nanoparticle-based muds has been investigated, while four TiO_2 nanoparticles with sizes of 5, 10, 15 and 50 nm have been used to conduct the tests. In all of the tests, the nanoparticle concentrations have been fixed at 0.5 wt%. Figure 5 shows the experimental results.

Measurements for different sizes of TiO_2 nanoparticle were within an average relative standard deviation of 5.3% for PV, 8.2% for YP, 7.2% for gel strength (10 min), 4.6% for n value, 5.5% for K value and 7.3% for YP/PV ratio, with 15 nm nanoparticle having the least relative standard deviation and 5 nm nanoparticle having highest relative standard deviation. Even though the experiments in this scenario are conducted at constant 25°C, still sometimes deviations in temperature are encountered during the experiment run. The reason for the better repeatability of 15 nm nanoparticle is due to a small difference in the temperatures of the two experiment runs. While for 5 nm nanoparticle, a difference of 2.3°C was observed between the two experiment runs, which would increase the amount of error.

As can be seen from Fig. 5 (a), the PV decreases with the increasing nanoparticle size, while the PVs of the muds composed of 15 and 50 nm nanoparticles are lower than those of the pure mud. These trends may be explained by the different electrical properties of the clay surface and TiO_2 nanoparticles. In general, the clay surface is negatively charged, while the surface of the TiO_2 nanoparticle is positively charged. Thus, adding TiO_2 nanoparticles into the mud may cause aggregation. Although aggregation may occur by adding TiO_2 nanoparticles, if the nanoparticle size is smaller, such as 5 and 10 nm in this study, the surface area to volume ratio of the solids in the nanoparticle-based muds may be still higher than that of the pure mud. This is why the PVs of the muds composed of 5 and 10 nm nanoparticles are higher than those of the pure mud (Li et al., 2012). With increasing nanoparticle size, more aggregation may occur, and the specific surface area (SSA) of the nanoparticles may decrease, as shown in Table 1, which both result in the reduction of the surface area to volume ratio of the nanoparticle-based muds. Thus, the PVs of the nanoparticle-based muds decrease with increasing nanoparticle size. Eventually, at a critical point, the surface area to volume ratio of the solids in the nanoparticle-based muds is lower than that of the pure mud, while accordingly, their PVs are lower than those of the base mud. It should be noted

that only the mud composed of 5 nm nanoparticle satisfies the API minimum PV value requirement.

As can be seen from Figs. 5 (b), (c) and (d), the YPs and gel strengths show similar trends by adding TiO_2 nanoparticles. In general, the YPs and gel strengths of the muds composed of TiO_2 nanoparticles are higher than those of the pure mud, since the TiO_2 nanoparticles are positively charged, increasing the attractive forces in the fluids (Loosli et al., 2015). However, the relationships among YPs and gel strengths and the nanoparticle size are not monotonic, while those may be attributed to the different amount of positive charge associated with the different size of nanoparticles. The 5 nm TiO_2 nanoparticle may be associated with the most positive charge, causing the largest attractive forces in the fluids, so its mud generates largest values of YPs and gel strengths. The 10 nm TiO_2 nanoparticle may be associated with the least positive charge, causing the smallest attractive forces in the fluids, so its mud generates minimum values of YPs and gel strengths.It can be observed from Fig. 5 (b) that the YPs of all the different sizes of TiO_2 nanoparticle satisfy the YP API requirement as they are lower than the maximum API value. Also, the different amounts of positive charge associated with the different sizes of nanoparticles can explain the non-monotonic change of YP/PV, n and K with nanoparticle size. In general, comparing the YP/PV, n and K values of the muds composed of TiO_2 nanoparticles with those of the base mud, the hole cleaning capacity can be improved by adding TiO_2 nanoparticles. Furthermore, it can be seen in Fig 5 (e) that muds composed of TiO_2 nanoparticles have YP/PV ratios less than the maximum API value. Hence, they satisfy the YP/PV ratio API requirement.

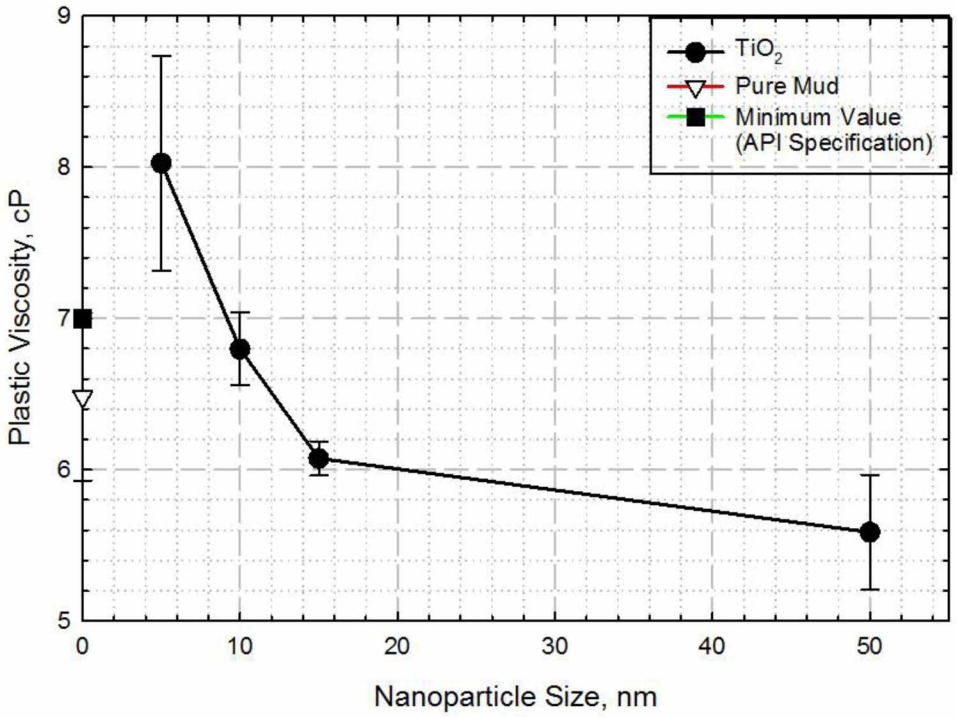

Figure 5 (a): Effect of Nanoparticle Size on Plastic Viscosity

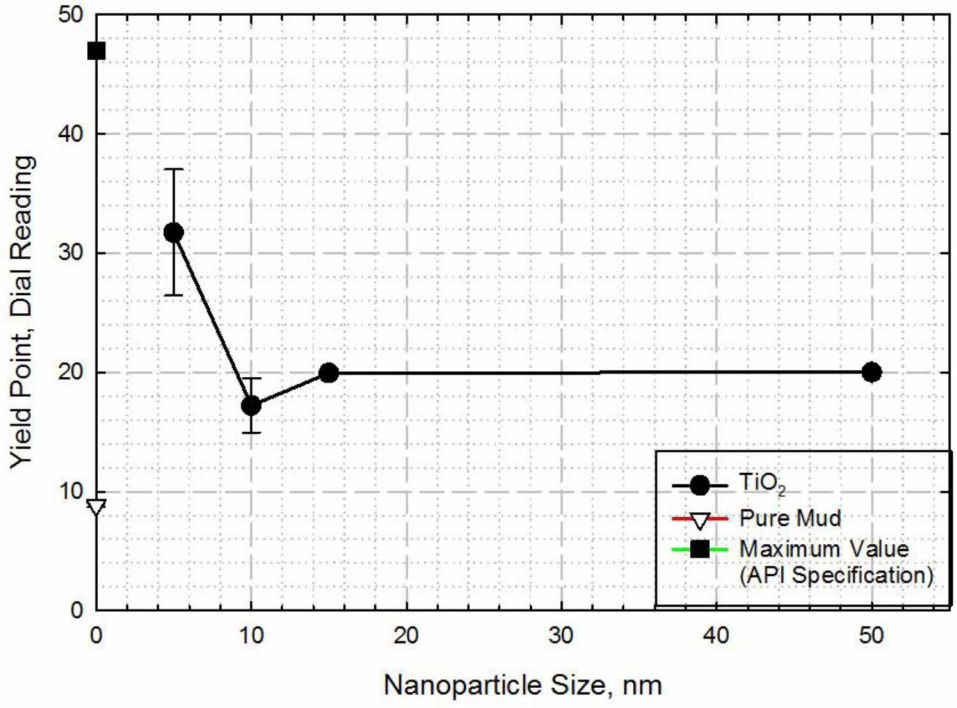

Figure 5 (b): Effect of Nanoparticle Size on Yield Point

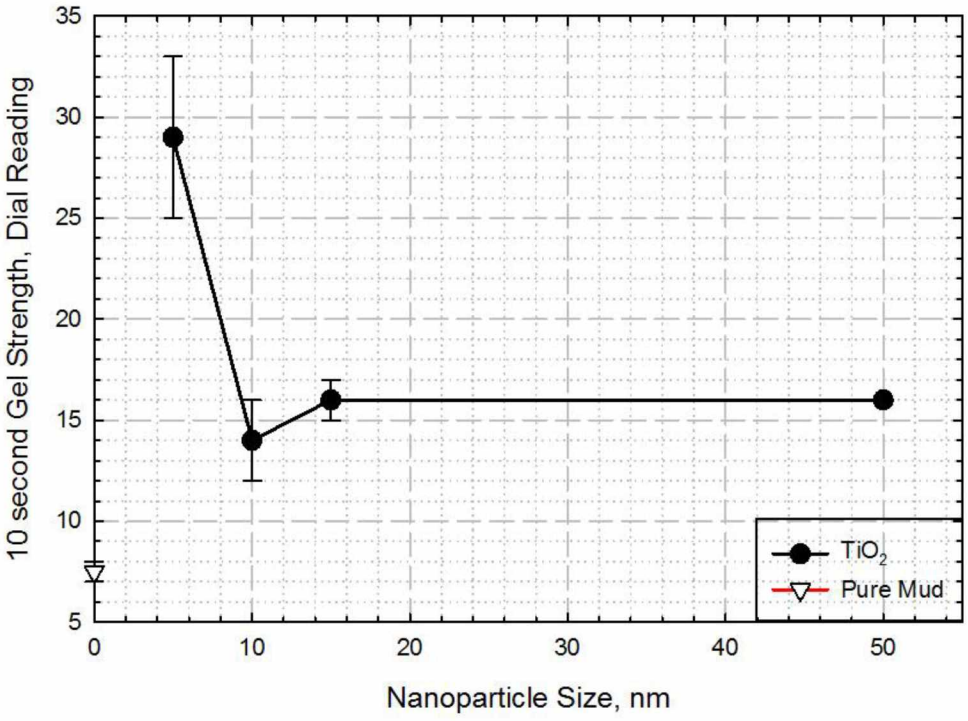

Figure 5 (c): Effect of Nanoparticle Size on 10 sec Gel Strength

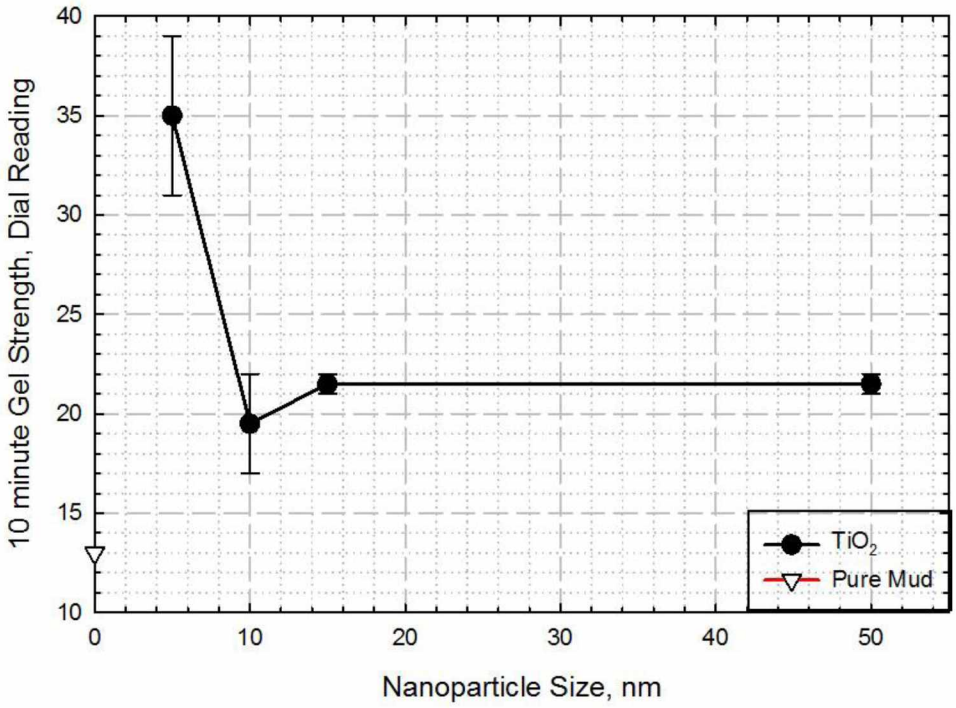

Figure 5 (d): Effect of Nanoparticle Size on 10 min Gel Strength

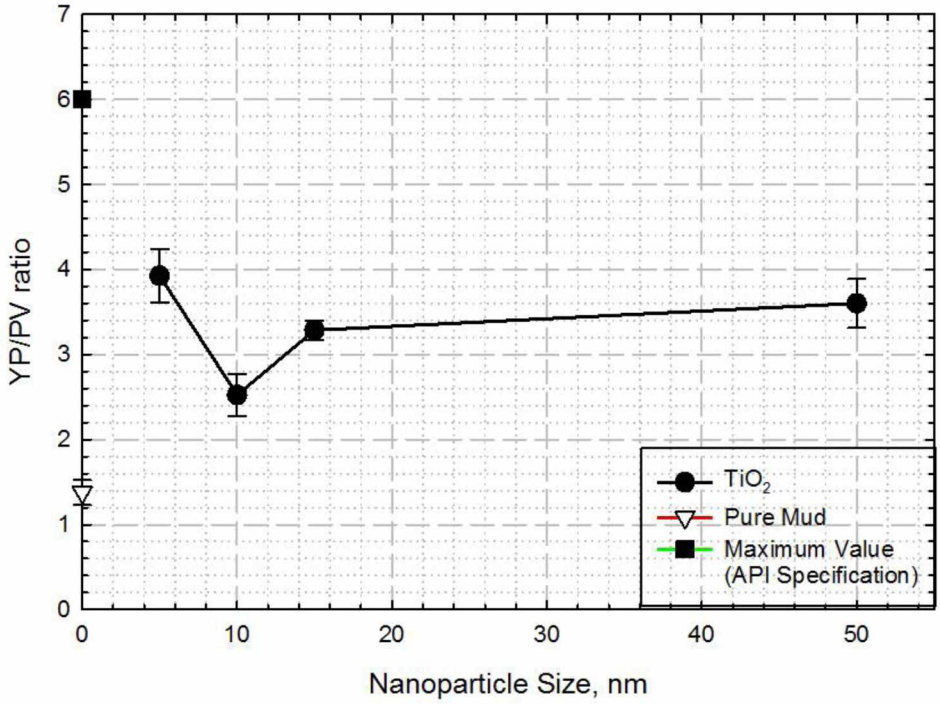

Figure 5 (e): Effect of Nanoparticle Size on YP/PV ratio

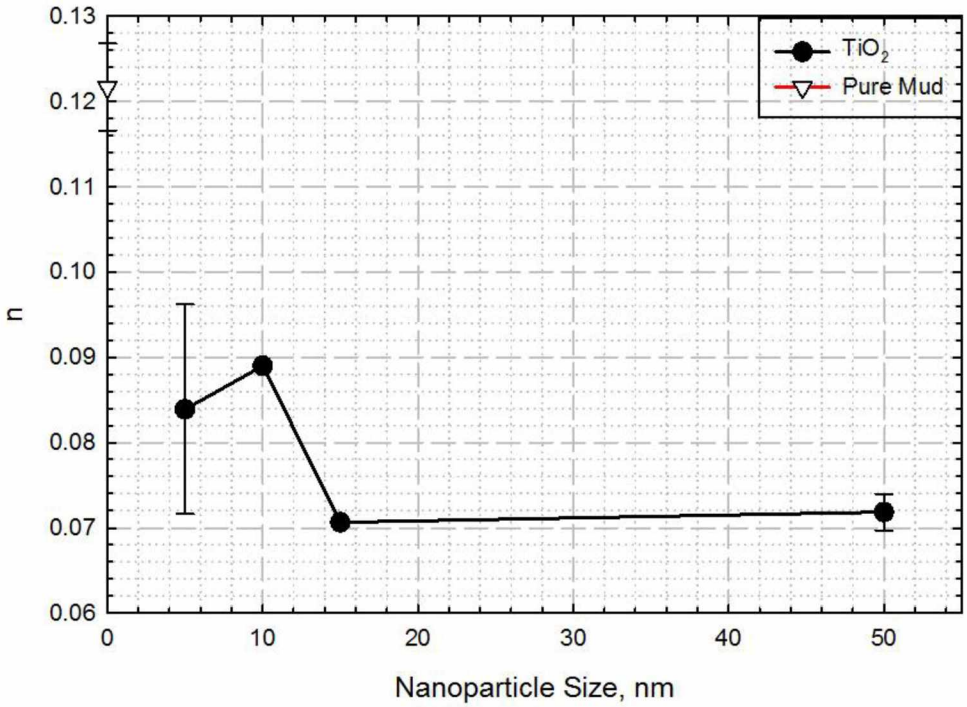

Figure 5 (f): Effect of Nanoparticle Size on Power Law Index

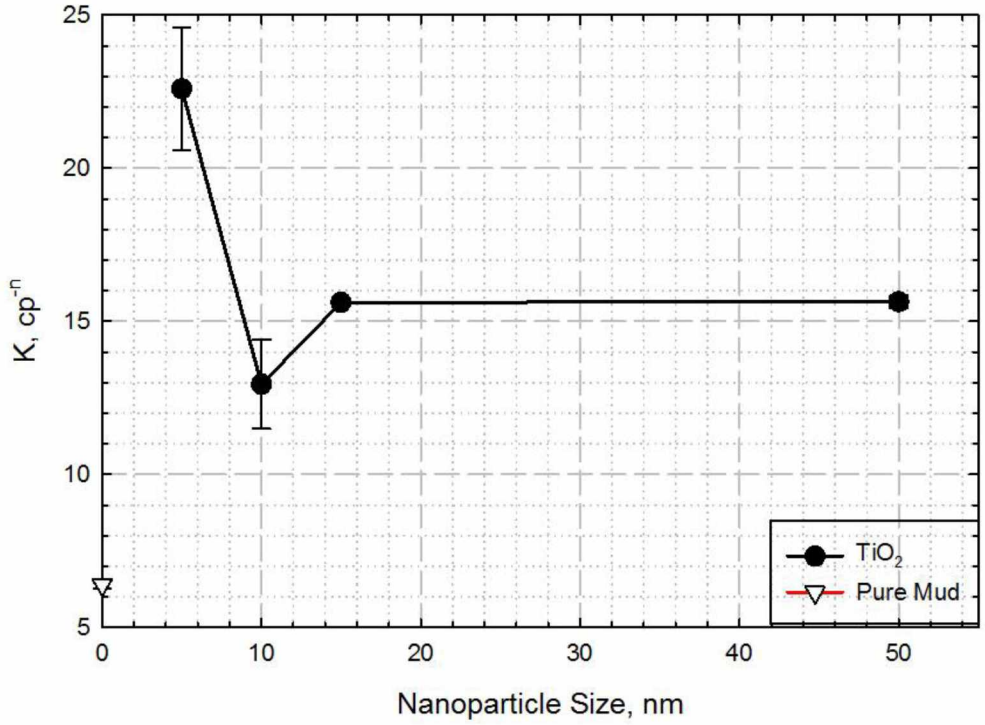

Figure 5 (g): Effect of Nanoparticle Size on Consistency Factor

4.1.3 Effect of Type

In this scenario, the influence of nanoparticle type on the rheological properties of nanoparticle-based muds has been investigated. This scenario used four different nanoparticles, namely Al_2O_3, Fe_3O_4 and two SiO_2 nanoparticles, one without any coating and other with KH550 coating. The Al_2O_3 nanoparticle is hydrophilic in nature and is known to have a high catalytic activity, while the Fe_3O_4 nanoparticle is also hydrophilic in nature and is superparamagnetic. All four types of nanoparticles have been tested at the concentration of 0.5 wt%, with the results presented in Fig. 6.

Measurements for SiO_2 with KH550 and SiO_2 without coating nanoparticles were within an average relative standard deviation of 8.6% and 0.9% for PV, 18.2% and 19% for YP, 7.2% and 6% for gel strength (10 min), 1.6% and 4% for n value, 2% and 3.7% for K value and 9% and 14% for YP/PV ratio, respectively. While, Fe_3O_4 nanoparticle measurements were within 2.3% for PV, 0.1% for YP, 0% for gel strength, 3.3% for n value, 0.8% for K value and 2.2% for YP/PV ratio.

The relative standard deviation for Al_2O_3 is zero as the measurements were carried out for only one set of experiment, due to its limited amount. The excellent repeatability of Fe_3O_4 nanoparticle is due to difference of only 0.07°C between the two experiment runs.

As can be seen from Fig. 6 (a), the plastic viscosity (PV) for nanoparticle-based muds is generally greater than that of the base mud, except for the Fe_3O_4 nanoparticle. The ascending order of increasing PV among the nanoparticles is Fe_3O_4, SiO_2 with KH550 coating, SiO_2 without coating, and Al_2O_3. Since the Fe_3O_4 nanoparticle has a high density, it will have fewer particles in dispersion compared to the others. Due to its high positive charge, it might cause particle aggregation, which could be the reason for its low PV value. The potential reason for the SiO_2 without coating nanoparticle to have higher PV than the SiO_2 coated with KH550 nanoparticle may be the latter's higher density. Hence, the SiO_2 without coating nanoparticle will have a higher number of particles in dispersion compared to the SiO_2 with KH550 coating nanoparticle. Further, the Al_2O_3 nanoparticle has the greatest specific surface area among all the different types of nanoparticles, which is reflected by its high PV value. Also, except for muds composed of Fe_3O_4 nanoparticle, other nanoparticle-based muds satisfy the minimum value for API PV requirement. As can be seen in Figs. 6 (b), (c) and (d), the yield points (YP) and gel strengths show a similar trend. The YP and gel strength values for both SiO_2 nanoparticles are quite low and similar. As both of the SiO_2 nanoparticles are negatively charged, their introduction into the mud will decrease the attractive forces and will lead to a decrease in YP and gel strength values. In this scenario, Al_2O_3 shows significantly higher YP and gel strength values than those of the rest of the nanoparticles. The likely explanation for this behavior may be its high specific surface area accompanied by the positive charge on the surface. Also, owing to its relatively low density in comparison to the Fe_3O_4 nanoparticle, it will have a higher number of positively charged particles in dispersion, which increases YP and gel strength values. Besides, the Fe_3O_4 nanoparticle also has a positive charge which will cause flocculation and result in an increase in YP and gel strength values. Furthermore, through Fig 6 (b) it can bee seen that Al_2O_3 nanoparticle-based mud has YP values higher than the maximum API YP value. Thus, it does not adhere to the standards requirement. While, other nanoparticle-based muds satify the YP API requirement.

The influence of nanoparticle type on YP/PV ratios, n values, and K values is described in Figs. 6 (e), (f), and (g), respectively. As can be seen, YP/PV ratios and K values decrease for both SiO_2

nanoparticles, while they increase for positively charged Al_2O_3 and Fe_3O_4 nanoparticles. However, n values increase for both the SiO_2 nanoparticles and decrease for the Al_2O_3 and Fe_3O_4 nanoparticles. Further, it can be observed from Figs. 6 (e), (f), and (g) that YP/PV ratios and K values for both SiO_2 nanoparticles are lower than those of the base mud, while they are higher for the Al_2O_3 and Fe_3O_4 nanoparticles. The n values are higher for both SiO_2 nanoparticles, while they are lower for the Al_2O_3 and Fe_3O_4 nanoparticles than the base mud. Therefore, compared to base mud, adding positively charged Al_2O_3 and Fe_3O_4 nanoparticles (at 5 wt%) can improve the mud's hole cleaning capacity, while addition of negatively charged SiO_2 nanoparticles (at 5 wt%) is detrimental to the mud's hole cleaning function. Also, even though Al_2O_3 nanoparticle-based mud does not conform to API YP requirement, it along with other nanoparticle-based muds satifies the YP/PV ratio API requirement.

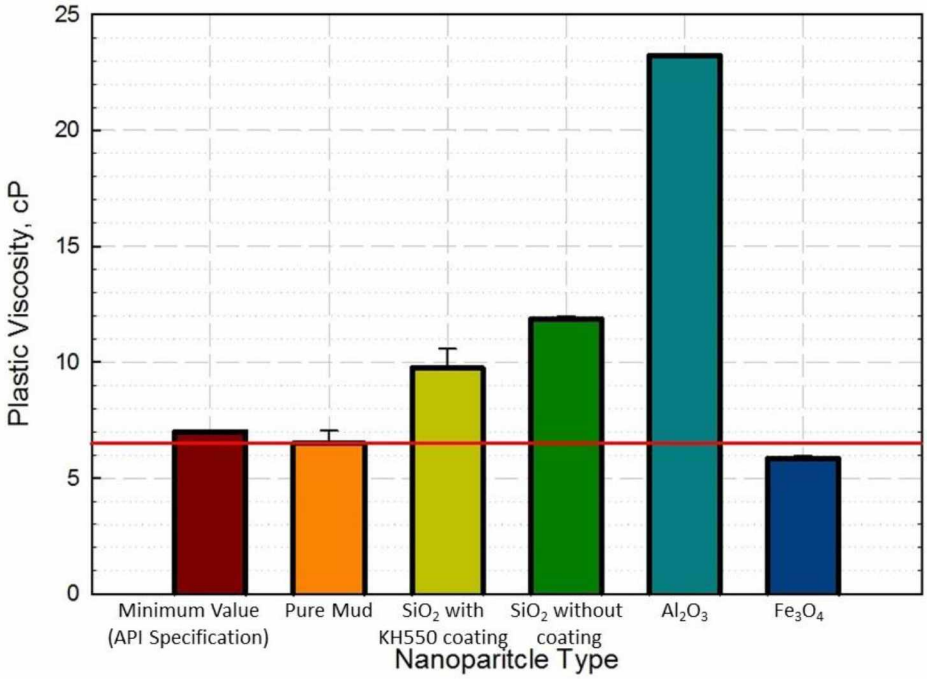

Figure 6 (a): Effect of Nanoparticle Type on Plastic Viscosity

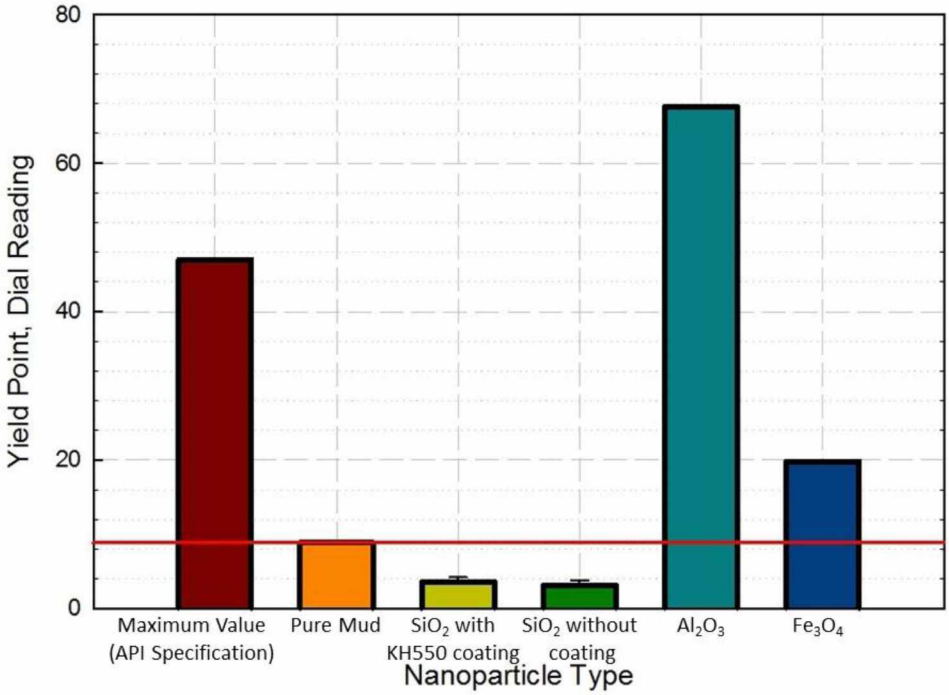

Figure 6 (b): Effect of Nanoparticle Type on Yield Point

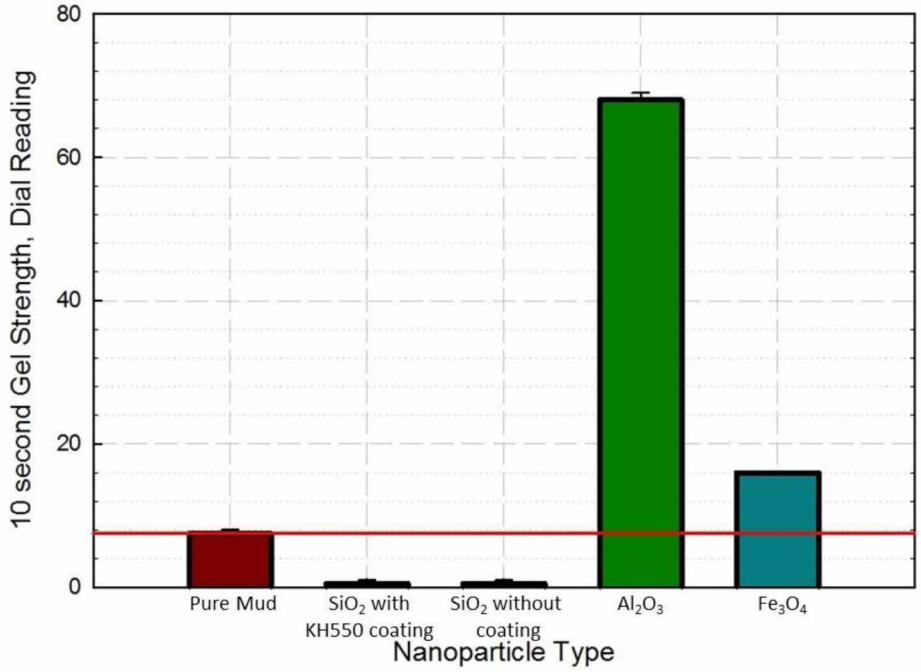

Figure 6 (c): Effect of Nanoparticle Type on 10 sec Gel Strength

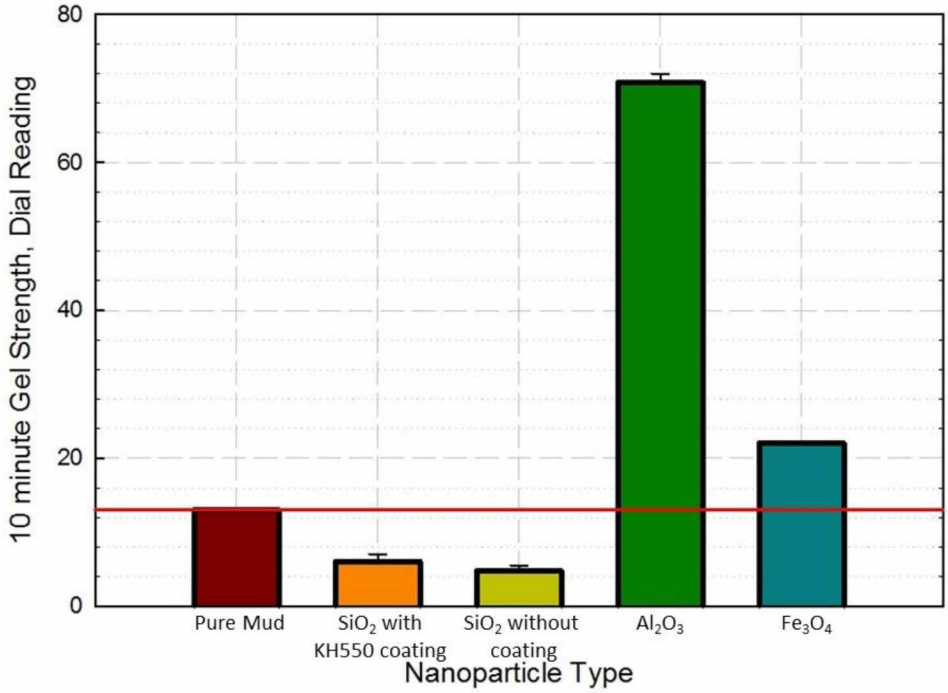

Figure 6 (d): Effect of Nanoparticle Type on 10 min Gel Strength

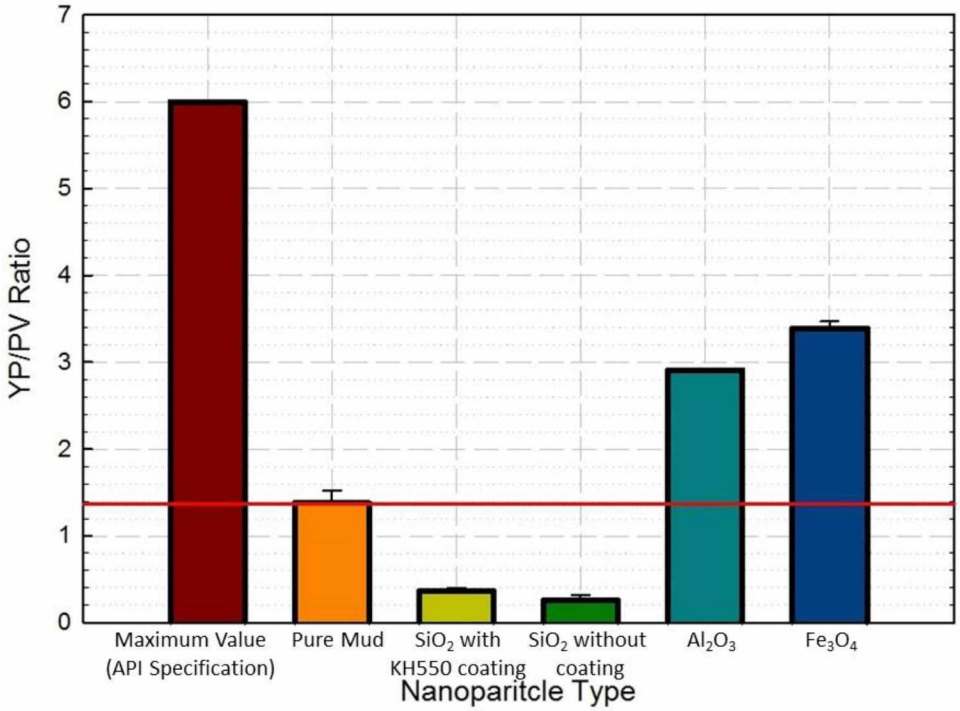

Figure 6 (e): Effect of Nanoparticle Type on YP/PV ratio

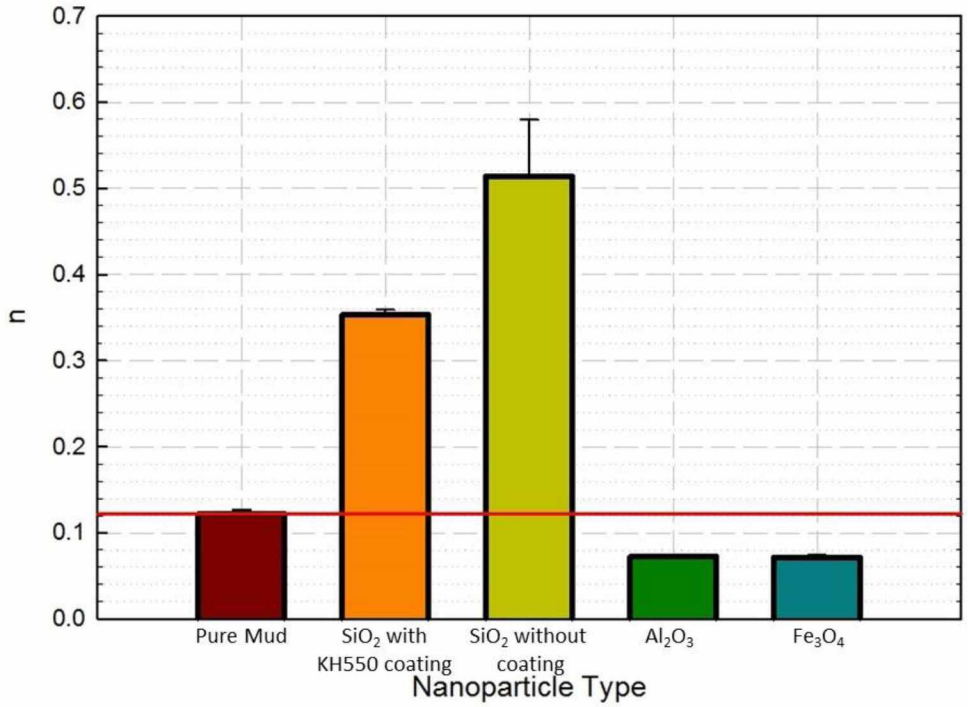

Figure 6 (f): Effect of Nanoparticle Type on Power Law Index

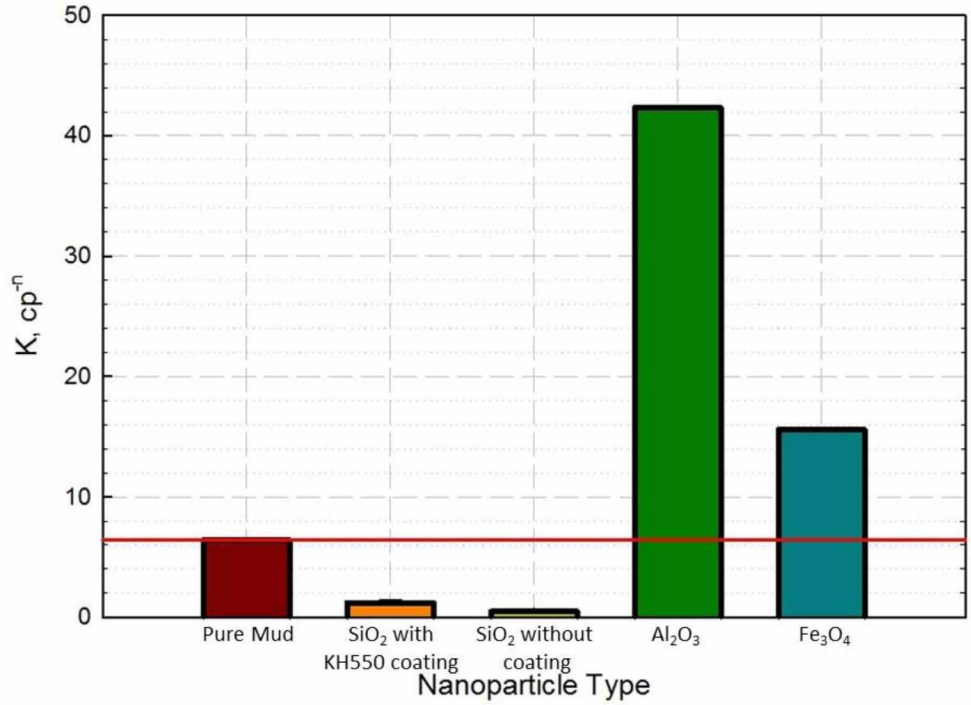

Figure 6 (g): Effect of Nanoparticle Type on Consistency Factor

4.1.4 Effect of Aging

In this scenario, the influence of aging on the rheological properties of nanoparticle-based muds has been investigated. This scenario used eight different nanoparticles, namely SiO_2 with KH550 coating, SiO_2 without coating, four different sizes of TiO_2 nanoparticles (5 nm, 10 nm, 15nm and 50 nm), Al_2O_3 and Fe_3O_4. All eight types of nanoparticles have been aged and tested at the concentration of 0.5 wt%, the results of which have been presented in Fig. 7.

Measurements for aged SiO_2 with KH550 and SiO_2 without coating nanoparticles were within an average relative standard deviation of 1.1% and 3.7% for PV, 0.9% and 7.1% for YP, 13% and 12% for gel strength (10 min), 2.1% and 4.2% for n value, 12% and 2.4% for K value and 6% and 2.8% for YP/PV ratio, respectively. While, measurements for aged different sizes of TiO_2 nanoparticle were within of 6.8% for PV, 5.5% for YP, 6.9% for gel strength, 5.6% for n value, 7.5% for K value and 9.3% for YP/PV ratio, with aged 5 nm nanoparticle having highest relative standard deviation. The reason for high relative standard deviation of aged TiO_2 15 nm nanoparticle is temperature fluctuations in the two experiment runs. The relative standard deviations for Al_2O_3 and Fe_3O_4 nanoparticles were zero as the measurements were carried out for only one set of experiment, due to their limited amount.

As can be seen from Fig. 7 (a), the plastic viscosity (PV) for nanoparticle-based muds is significantly affected by the aging process. In the case of the base mud, aging leads to increase in PV. This may be explained by dissociation of clay particles at elevated temperatures. With exposure to high temperature, the face-to-face and face-to edge associations might break down among the clay particles, leading to increased PV. For both SiO_2 nanoparticles, aging causes increased PV, which may be due to the combined effects of dissociation and slight flocculation caused by negatively charged SiO_2 nanoparticles. The increase in PV is greater for the SiO_2 without coating nanoparticle compared to the one with KH550 coating, due to the presence of more particles in dispersion by the former. However, after aging, the TiO_2 5 nm and Al_2O_3 nanoparticles show a reduction in PV, which may be attributed to their positive charge and high specific surface area, and may lead to aggregation among the particles. Further, after aging, the TiO_2 10 nm, TiO_2 15 nm, TiO_2 50 nm and Fe_3O_4 nanoparticles show increased PV, which may be explained by the dissociation of clay particles. Except for aged TiO2 5 nm, the other aged nanoparticle-based muds satisfy the minimum API PV requirement. As can be seen from Figs. 7 (b), (c) and (d), the yield

points (YP) and gel strengths show a relatively similar trend. After aging, the base mud's YP and gel strength values decrease. This can be explained by dissociation of clay particles at elevated temperatures resulting in a number of negatively charged clay particles, which repel each other and thus reduce the attractive forces. Both SiO_2 nanoparticles show an increase in YP and gel strength values, which may be recognized by flocculation caused by them. In addition, the TiO_2 5 nm, TiO_2 10 nm, TiO_2 15 nm, TiO_2 50 nm, Al_2O_3 and Fe_3O_4 nanoparticles show a reduction in YP and gel strength values after aging. A potential reason for this behavior could be that the number of dissociated clay particles is significantly greater and overcomes the number of positively charged nanoparticles and leads to a net repulsive force which reduces the YP and gel strength values. Also, it can be seen from Fig. 7 (b) that except for aged Al_2O_3 nanoparticle-based muds, the other nanoparticle-based muds have YP less than the specified maximum API YP value. Thus, except for aged Al_2O_3 nanoparticle, the other nanoparticle-based muds satisfy the API YP standard.

The influence of aging on YP/PV ratios, n values, and K values is shown in Figs. 7 (e), (f), and (g), respectively. As can be observed, after aging, YP/PV ratios and K values decrease for both pure mud and nanoparticle-based mud, while the n values generally increase after aging. This indicates that aging has an adverse effect on the mud's hole cleaning function. However, if we contrast the hole cleaning capacity of nanoparticle-based muds with aged base mud, it can be seen in Figs. 7 (e), (f), and (g) that aged TiO_2 5 nm, TiO_2 10 nm, TiO_2 15 nm, TiO_2 50 nm, Al_2O_3 and Fe_3O_4 have YP/PV ratios and K values higher than those of the aged base mud. The n values of aged TiO_2 5 nm, TiO_2 10 nm, TiO_2 15 nm, TiO_2 50 nm, Al_2O_3 and Fe_3O_4 are lower than those of the aged base mud. This indicates that aged TiO_2 5 nm, TiO_2 10 nm, TiO_2 15 nm, TiO_2 50 nm, Al_2O_3 and Fe_3O_4 can improve the mud's hole cleaning capacity compared to aged base mud. It can also be observed that all the aged muds have YP/PV ratios less than the maximum API value. Thus, all of them satify the API YP/PV ratio requirement.

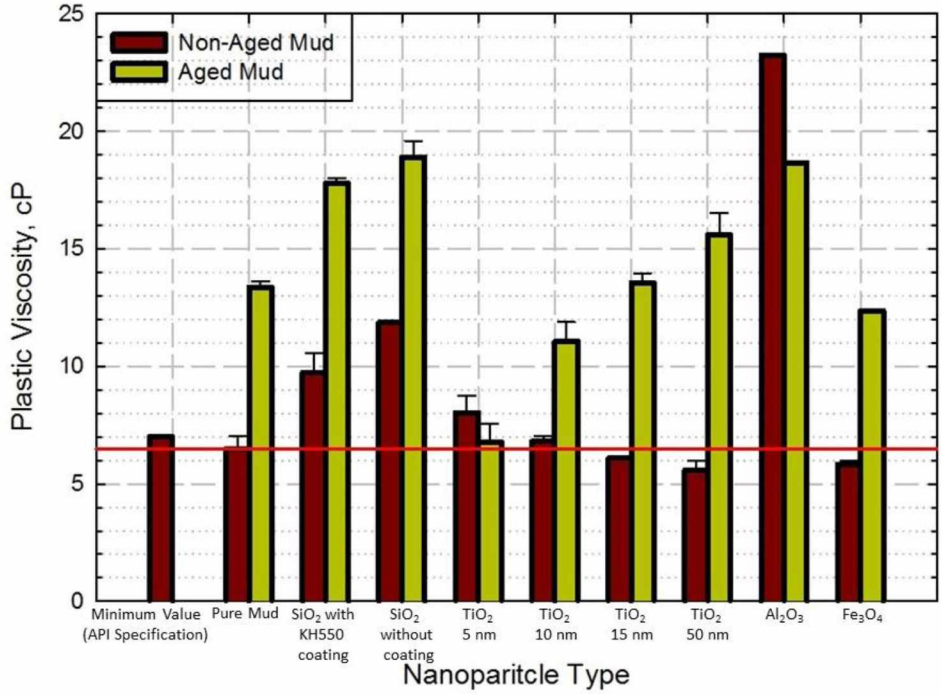

Figure 7 (a): Effect of Aging on Plastic Viscosity

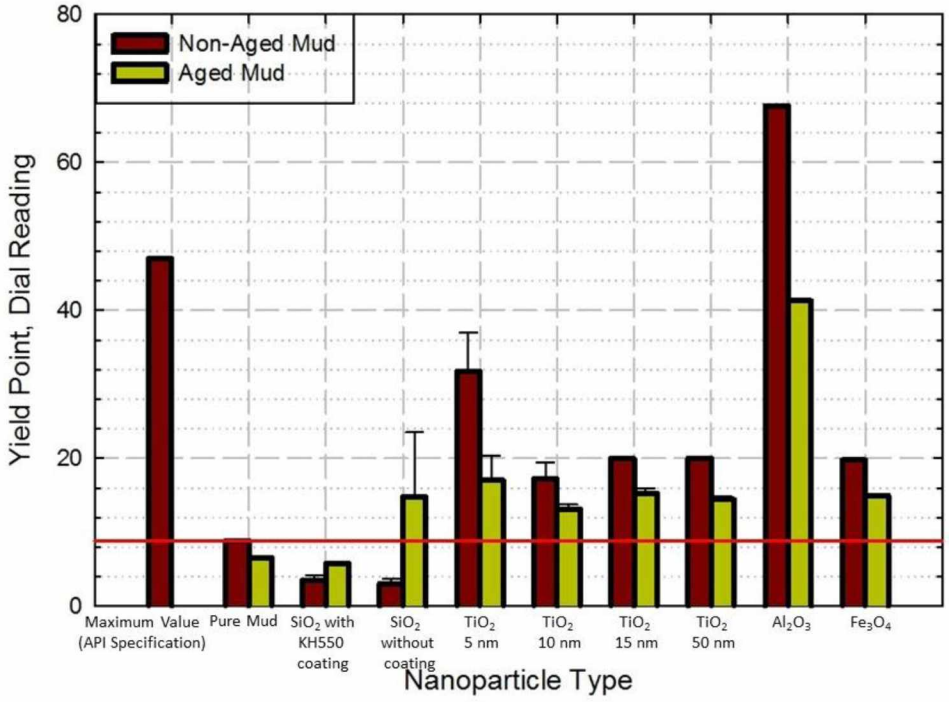

Figure 7 (b): Effect of Aging on Yield Point

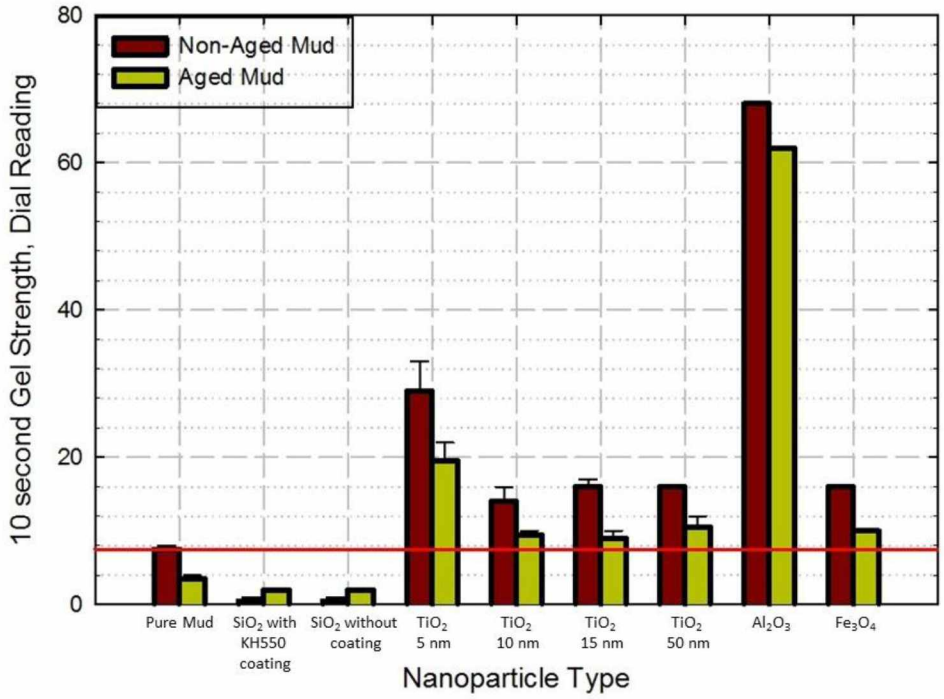

Figure 7 (c): Effect of Aging on 10 sec Gel Strength

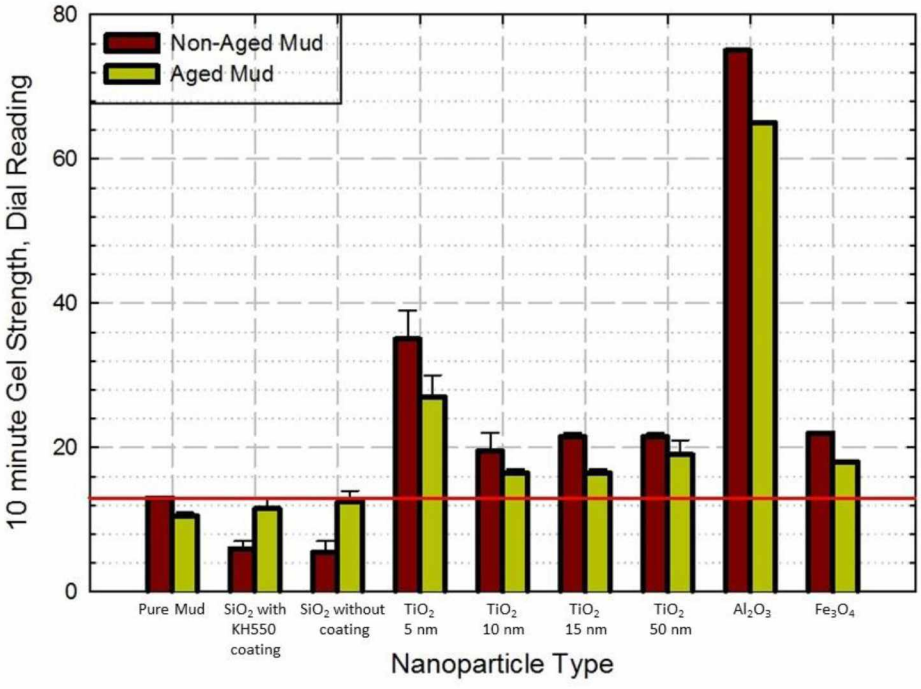

Figure 7 (d): Effect of Aging on 10 min Gel Strength

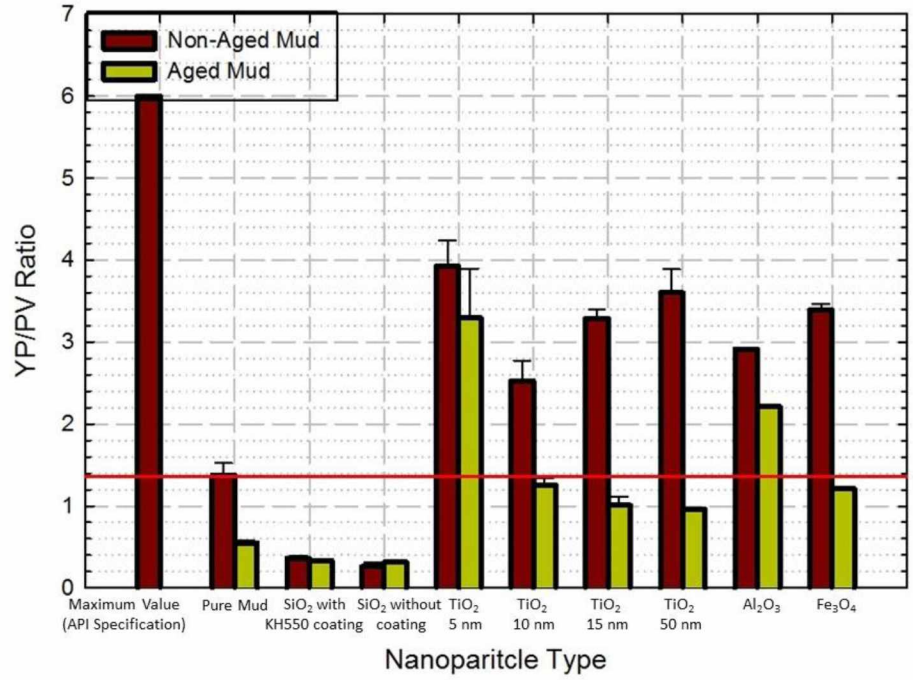

Figure 7 (e): Effect of Aging on YP/PV ratio

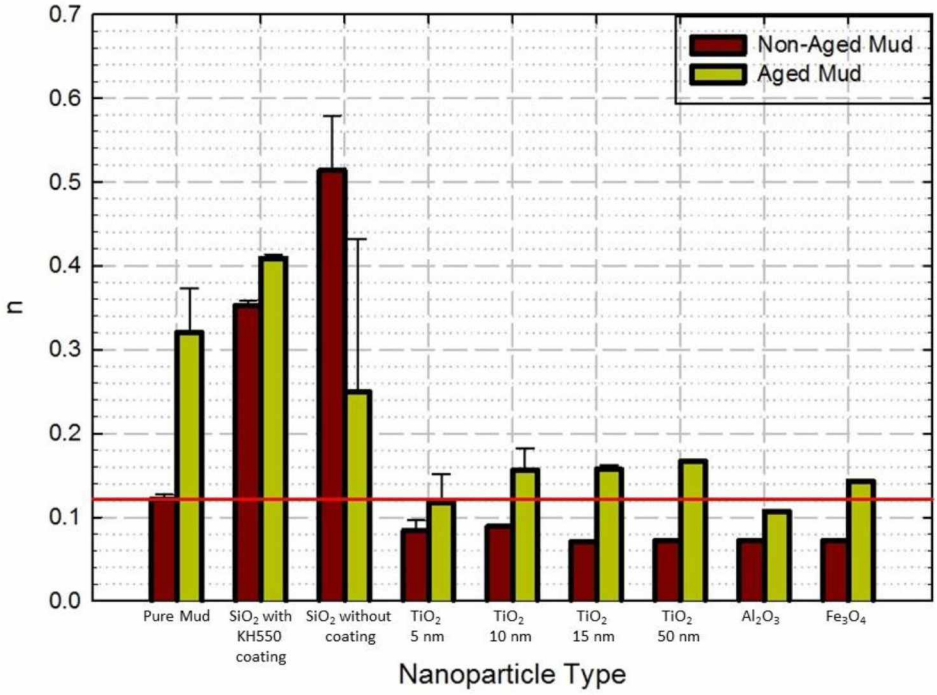

Figure 7 (f): Effect of Aging on Power Law Index

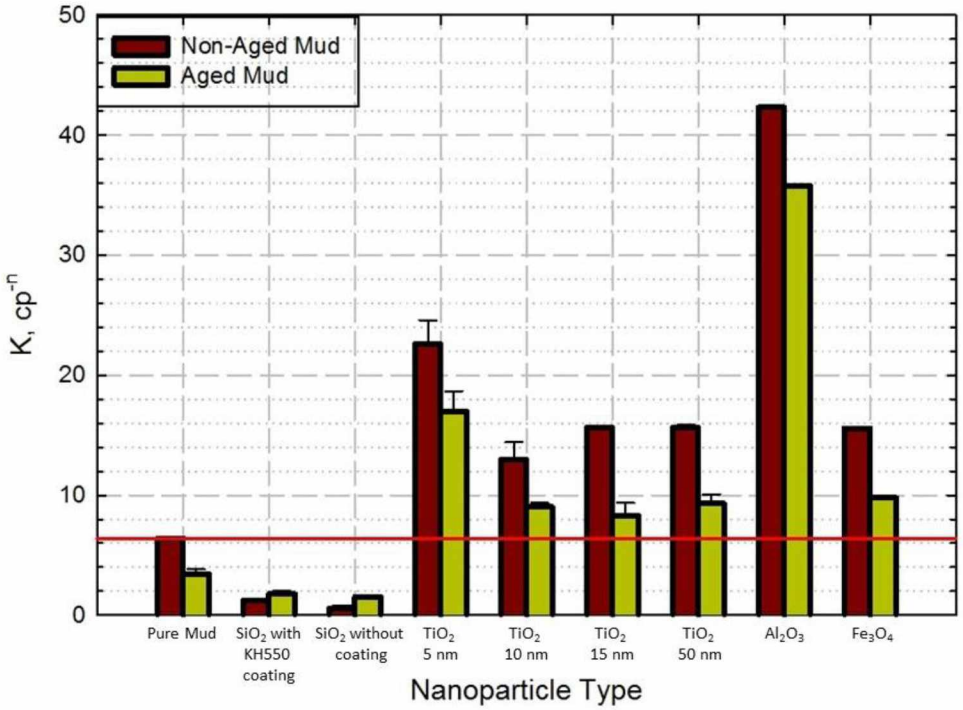

Figure 7 (f): Effect of Aging on Consistency Factor

4.1.5 Effect of Temperature

In this scenario, the influence of temperature on the rheological properties of nanoparticle-based muds has been investigated. Both of the nanoparticles used in this scenario are SiO_2, namely SiO_2 without coating nanoparticle and SiO_2 with KH550 coating. Both the nanoparticles are taken at a concentration of 0.5 wt% and have been tested at temperatures of 25, 40, 60 and 80°C, the results of which have been presented in Fig. 8.

For base mud, SiO_2 with KH550 coating and SiO_2 without coating nanoparticles, the relative standard deivation values for the measurements have been averaged for all the different temperatures to represent the average relative standard deviation for each rheological property. Measurements at different temperatures for base mud, were within an average relative standard deviation of 5.9% for PV, 1.4% for YP, 1% for gel strength (10 min), 9.6% for n value, 6.2% for K value and 1.7% for YP/PV ratio, with 80°C measurement having highest relative standard deviation due to temperature fluctuations between the two measurements. While, measurements

at different temperatures of SiO_2 with KH550 and SiO_2 without coating nanoparticles were within an average relative standard deviation of 11.5% and 0.3% for PV, 3.9% and 1.8% for YP, 6.1% and 7.6% for gel strength, 0.9% and 5.7% for n value, 1.6% and 14.4% for K value and 10.1% and 7.1% for YP/PV ratio, respectively. For both the nanoparticle highest relative standard deviation is associated with 80°C measurements, which is due to not maintaining a constant temperature when measurements are going on.

As can be seen from Fig. 8 (a), the plastic viscosity (PV) decreases with increasing temperature, which may be due to a partial destruction of the hydration clay suspensions, causing aggregation of particles, which would decrease the number of particles in dispersion and result in PV reduction (Sami, 2015). Furthermore, the PV decrease rate of the mud composed of the SiO_2 with KH550 coating nanoparticle is higher than that of the mud consisting of the SiO_2 without coating nanoparticle, since the SiO_2 with KH550 coating nanoparticle has a higher density than SiO_2 without coating nanoparticle, so the former will have fewer particles in dispersion compared to the latter. As PV depends upon the number of particles in dispersion, the SiO_2 without coating nanoparticle will have higher PV than the SiO_2 with KH550 coating nanoparticle. It can be observed that SiO_2 without coating nanoparticle has PV values greater than the minimum API PV requirement at all the tested temperatures. While, SiO_2 without coating nanoaprticle can satisfly the minimum API PV requirement upto 40°C, after which its PV values are lower than the minimum API PV requirement. As can be seen from Figs. 8 (b), (c) and (d), the yield points (YP) and gel strengths increase with increasing temperature for both SiO_2 nanoparticles and base mud. Besides, the increases in YP and gel strength are greater in the base mud than in the nanoparticle-based muds. A potential reason for this behavior could be higher flocculation in the base mud compared to nanoparticle-based muds. Both SiO_2 nanoparticles are negatively charged and would have less attractive force at ambient temperature. However, with an increase in temperature, negatively charged SiO_2 nanoparticles could come into contact with the positively charged edges of the clay particles, which could lead to flocculation, in turn increasing YP and gel strength. The SiO_2 with KH550 coating nanoparticle has a higher rate of increase in YP and gel strength compared to the SiO_2 without coating nanoparticle. The potential reason for this behavior could be the presence of a higher negative charge on the former nanoparticle due to its association with a silane coating. Also, both nanoparticle-based muds satisfy the API YP standard as they have YPs less than the maximum API YP requirement.

The influence of temperature on YP/PV ratios, n values, and K values is shown in Figs. 8 (e), (f), and (g), respectively. As can be observed, with increasing temperature, YP/PV ratios increase, n values decrease, and K values increase for both nanoparticles. It can be observed that the n values for both nanoparticles are greater than those of the base mud, while the YP/PV ratios and K values are less than those of the base mud. Thus, increasing temperature has an adverse effect on the nanoparticle-based mud's hole cleaning function. The base mud has YP/PV ratio greater than the maximum API requirement beyond 60°C. While, both the nanoparticle-based muds have YP/PV ratios less than the maximum API YP/PV requirements at all the tested temperatures, and so satisfy the API requirement.

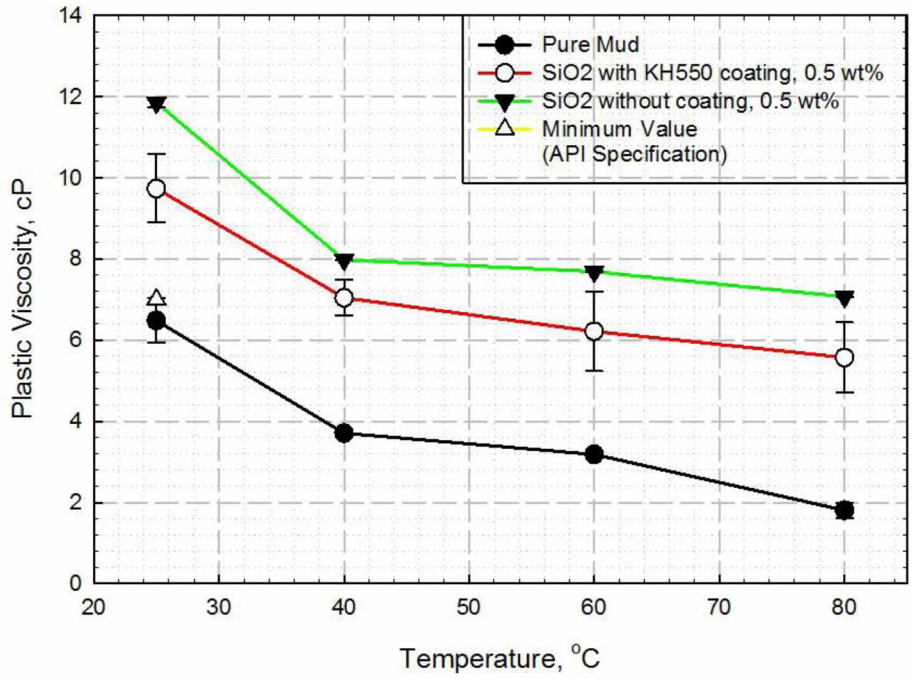

Figure 8 (a): Effect of Temperature on Plastic Viscosity

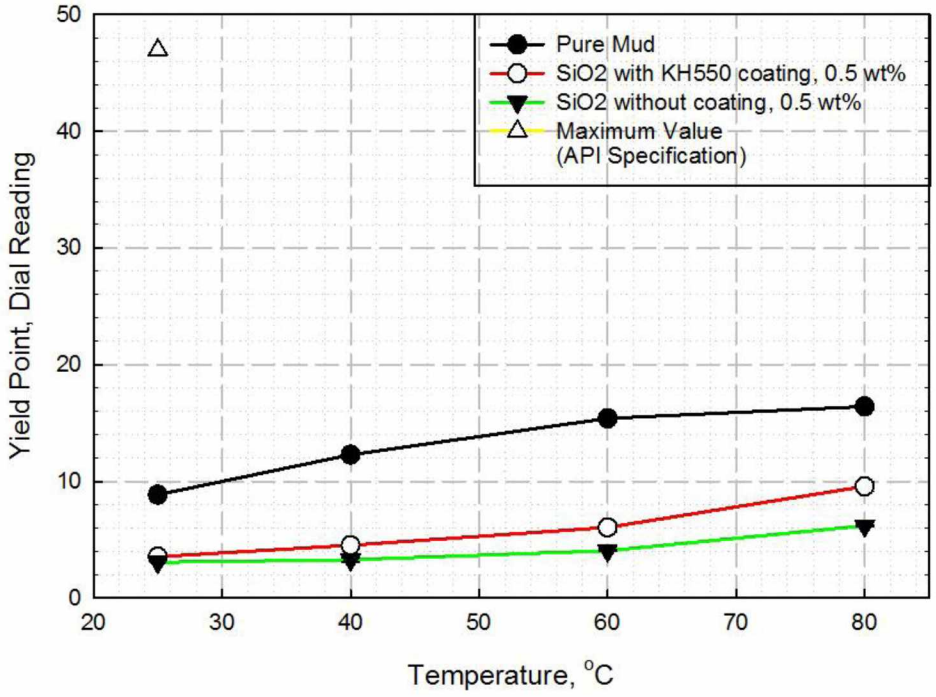

Figure 8 (b): Effect of Temperature on Yield Point

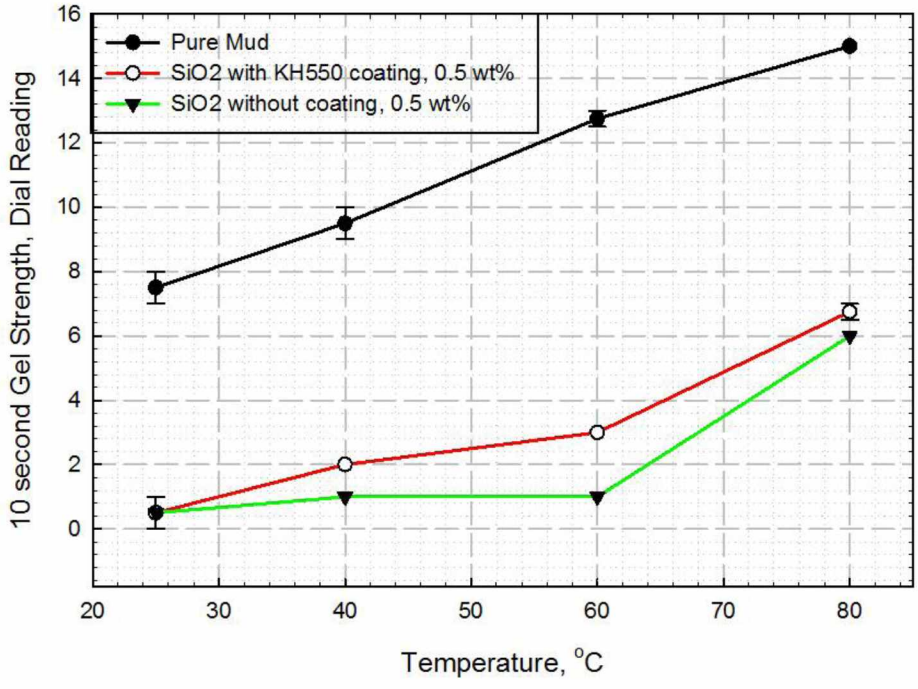

Figure 8 (c): Effect of Temperature on 10 sec Gel Strength

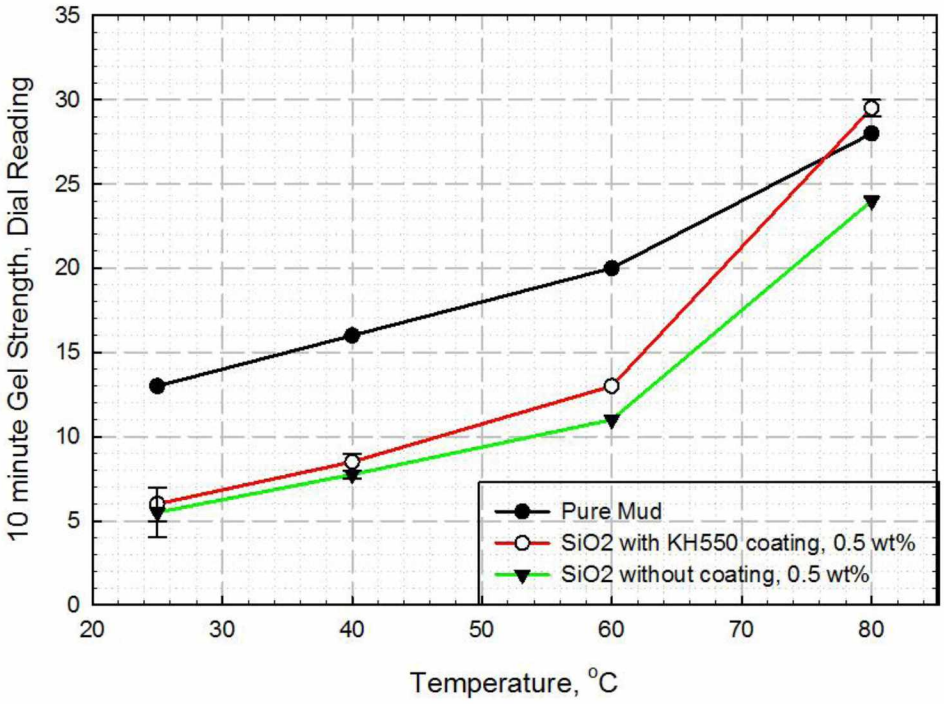

Figure 8 (d): Effect of Temperature on 10 min Gel Strength

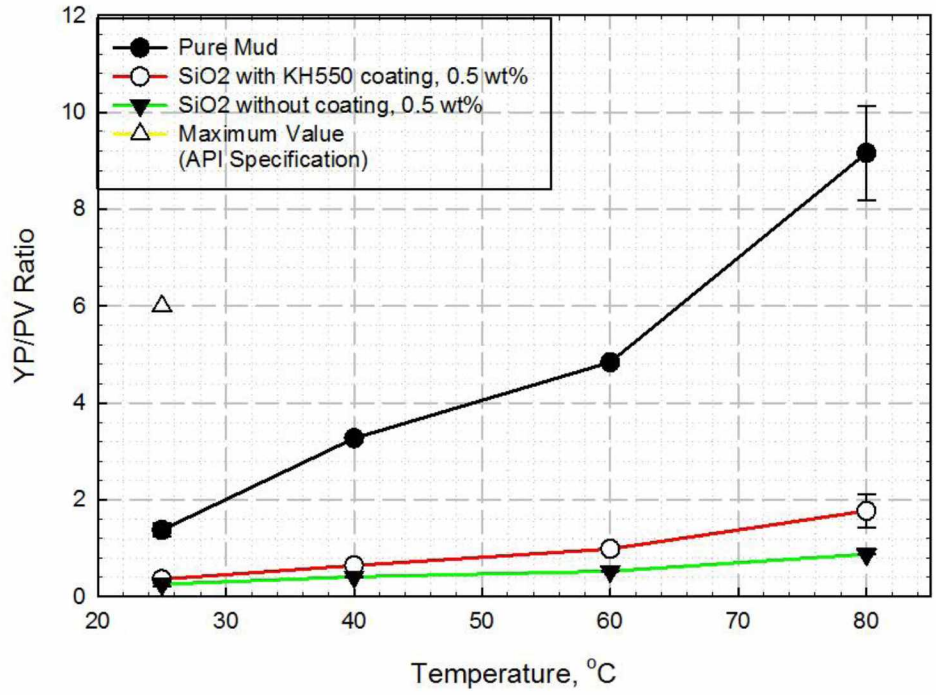

Figure 8 (e): Effect of Temperature on YP/PV ratio

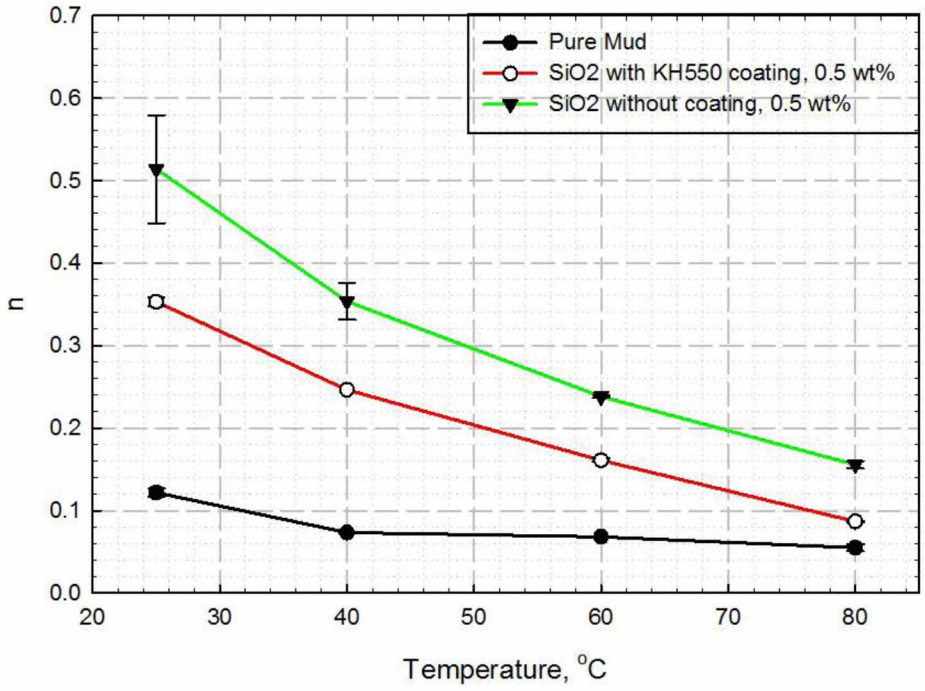

Figure 8 (f): Effect of Temperature on Power Law Index

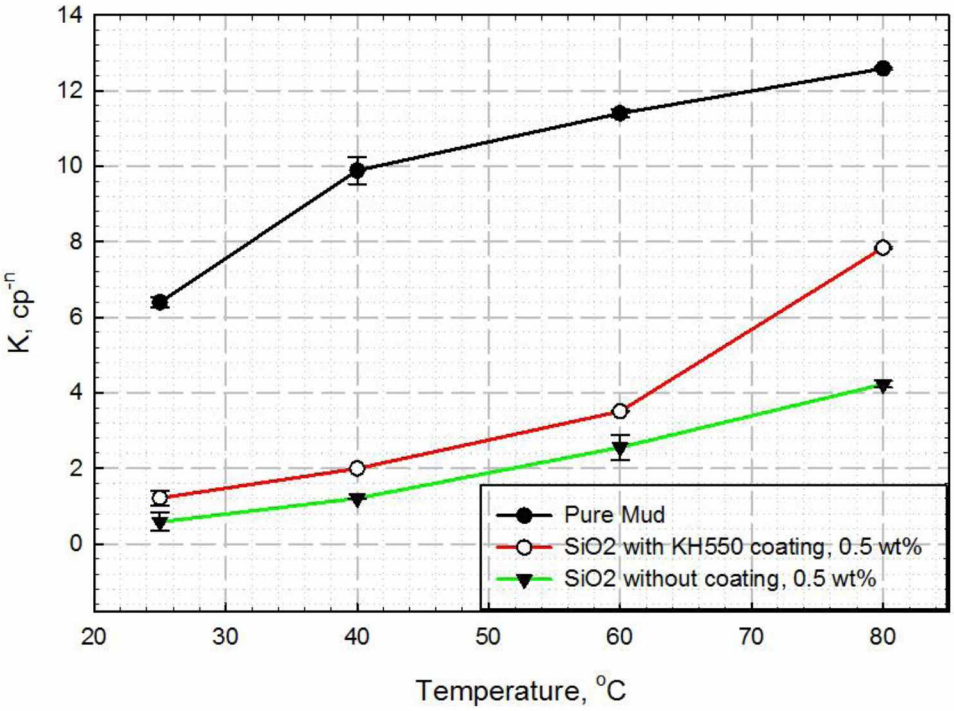

Figure 8 (g): Effect of Temperature on Consistency Factor

4.2 The Influence on Lubricity

In this subsection, the effects of nanoparticle concentration, nanoparticle size, nanoparticle type and aging on the lubricity of the nanoparticle-based muds have been investigated, while experimental results have been reported, analyzed and discussed. Also, the lubricity coefficient of the nanoparticle-based muds has been compared to the API specification.

4.2.1 Effect of Concentration

In this scenario, the influence of nanoparticle concentration on lubricity of nanoparticle-based muds has been investigated. Both of the nanoparticles used in this scenario are SiO_2, one without any coating and the other with KH550 coating. Lubricity coefficients have been measured for both nanoparticles at concentrations of 0.01, 0.05, 0.1, 0.25, 0.5 and 1 wt%, the results of which are presented in Fig. 9.

Lubricity coefficient measurements for SiO_2 with KH550 nanoparticle were within an average relative standard deviation of 3.5%. While, SiO_2 without coating nanoparticle measurements were within 5.2%. As can be seen in Fig. 9, the lubricity coefficient increases as nanoparticle concentration increases because the solid content of the drilling muds continues to increase with increasing nanoparticle concentration. Also, it is well known that increasing surface area of the solids increases the amount of friction of the drilling mud (Redburn et al., 2013). As the nanoparticle concentration increases, the total surface area of the nanoparticles increases, which consequently increases the amount of friction. In Fig. 9, it can also be observed that the increase in the lubricity coefficient is greater for the SiO_2 without coating nanoparticle than for the SiO_2 with KH550 coating nanoparticle. A potential reason for this behavior could be the presence of the coating on the SiO_2 with KH550 coating nanoparticle, which may reduce its size degradation. Also, at any given nanoparticle concentration, SiO_2 without coating nanoparticle has higher particles in mud compared to SiO_2 with KH550 coating nanoparticle. Besides, it can be seen that the lubricity coefficient values of the nanoparticle-based muds are lower than those of the base mud at lower nanoparticle concentrations (< 0.1 wt%). This amounts to improvements of 9.66% and 6.03% for the SiO_2 with KH550 coating nanoparticle, and 4.83% and 1.69% for the SiO_2 without coating nanoparticle, at concentrations of 0.01 wt% and 0.05 wt%, respectively. Thus, compared with the base mud, adding a small amount of SiO_2 nanoparticles (< 0.1 wt%) can

improve the mud's lubricity, while higher SiO_2 nanoparticle concentration (> 0.1 wt%) reduces the mud's lubricity. However, at all the tested nanoparticle concentrations, both nanoparticle-based muds have significantly higher lubricity coefficeients than the API requirement. Therefore, both nanoparticle-based muds do not meet the API lubricity requirement.

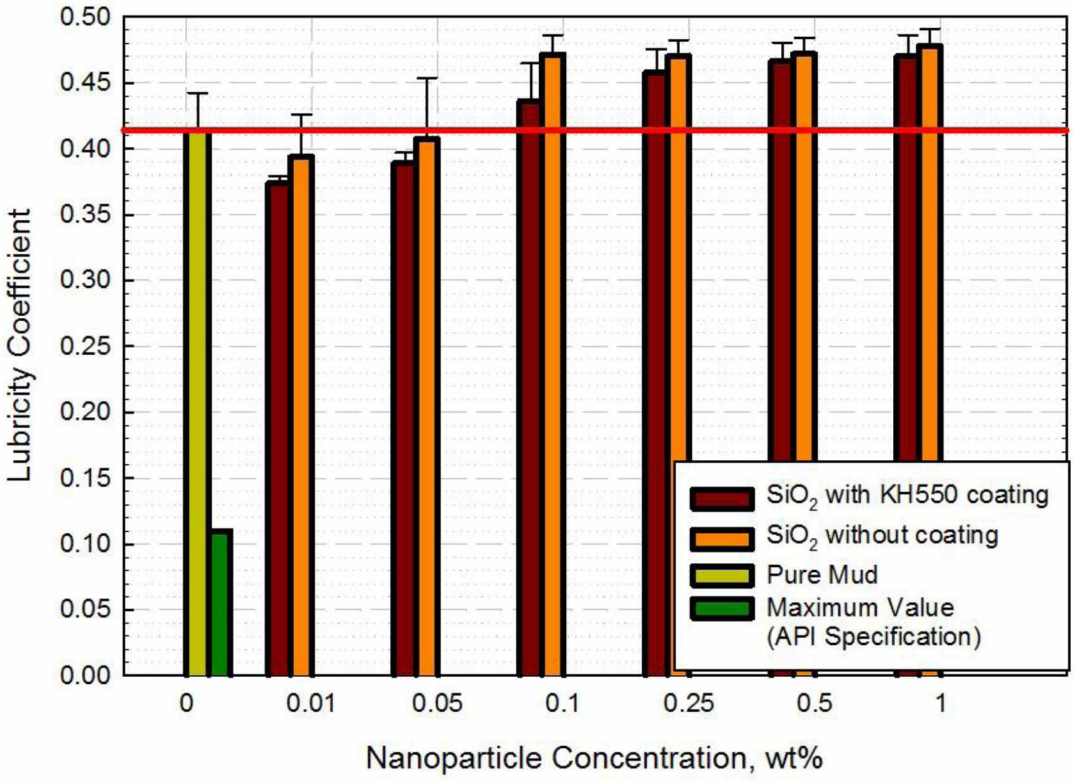

Figure 9: Effect of Nanoparticle Concentration on Lubricity Coefficient

4.2.2 Effect of Size

In this scenario, the influence of nanoparticle size on the lubricity of nanoparticle-based muds has been investigated. For this scenario, TiO_2 nanoparticles were tested at four different sizes of 5, 10, 15 and 50 nm, at the concentration of 0.5 wt%, while the results of which are presented in Fig. 10.

Lubricity coefficient measurements for different sizes of TiO_2 nanoparticle were within relative standard deviation of 1.1% for 5 nm, 0.4% for 10 nm, 0.8% for 15 nm and 3.7% for 50 nm. Indicating good repeatability for all the tested TiO_2 sizes. As can be seen in Fig. 10, the lubricity coefficient of nanoparticle-based muds decreases as nanoparticle size increases until 15 nm. Also, it can be observed that a further increase in nanoparticle size to 50 nm increases the lubricity coefficient. The decrease in lubricity coefficient until nanoparticle size of 15 nm may be explained by the reduction in the surface area of the nanoparticle with increasing nanoparticle size. However, at a nanoparticle size of 50 nm, the lubricity coefficient increases as the number of particles in suspension may increase due to size degradation of the 50 nm nanoparticles. Through Fig. 10, it can be observed that the lubricity coefficients for nanoparticle-based muds are greater than those for the base mud, indicating that, compared to the base mud, the addition of different sizes of the TiO_2 nanoparticle at a concentration of 0.5 wt% cannot improve the lubricity of the mud. Also, lubricity coefficient for nanoparticle-based muds is greater than the maximum API value for lubricity coefficient. Thus, TiO_2 nanoparticle-based muds do not satisfy the API lubricity requirement.

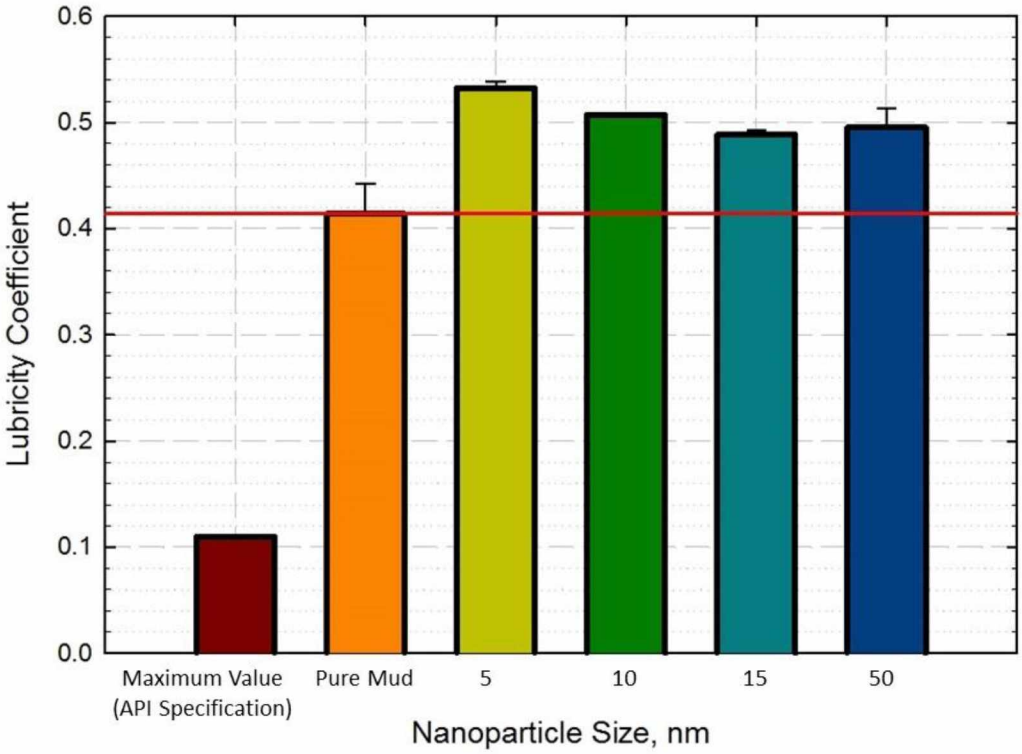

Figure 10: Effect of Nanoparticle Size on Lubricity Coefficient

4.2.3 Effect of Type

In this scenario, the influence of nanoparticle type on the lubricity of nanoparticle-based muds has been investigated. In this scenario, four different nanoparticles, namely Al_2O_3, Fe_3O_4 and two SiO_2 nanoparticles, one without any coating and other with KH550 coating, have been tested at a concentration of 0.5 wt%, the results of which have been presented in Fig. 11.

Lubricity coefficient measurements for SiO_2 with KH550, SiO_2 without coating, Al_2O_3 and Fe_3O_4 nanoparticles were within relative standard deviation of 3.1%, 2.6%, 1.4% and 0.6%, respectively. Indicating, good repeatability for all the tested nanoparticle types. As can be seen from Fig. 11, the lubricity coefficient for nanoparticle-based muds is greater than that of the base mud. The ascending order of increasing lubricity coefficient among the nanoparticles is Fe_3O_4, SiO_2 with KH550 coating, SiO_2 without coating and Al_2O_3. A potential reason for the Fe_3O_4 nanoparticle having a lubricity coefficient similar to that of the base mud may be its low specific surface area, high bulk density and positive charge. Owing to its high bulk density, the Fe_3O_4 nanoparticle will

have fewer particles in suspension compared to other types of nanoparticles, also due to its surface being positively charged, it will cause particle aggregation. Thus providing less friction compared to other nanoparticles. The lubricity coefficient of the SiO_2 with KH550 coating nanoparticle is lower than SiO_2 without coating nanoparticle due to the presence of the coating on the former, which protects against size degradation, thus reducing its lubricity coefficient in comparison. In this scenario, the Al_2O_3 nanoparticle exhibits a higher lubricity coefficient than other nanoparticles due to the fact that it has higher specific surface area, leading it to have greater friction and subsequently a higher lubricity coefficient. In this scenario, as the lubricity coefficient of nanoparticle-based muds is greater than that of the base mud, the addition of different nanoparticles at a concentration of 0.5 wt% has adverse effects on the drilling mud's lubricity. Also, lubricity coefficient for different nanoparticle-based muds is greater than the maximum API value for lubricity coefficient. Thus, the tested different types of nanoparticle-based muds do not satisfy the API lubricity requirement.

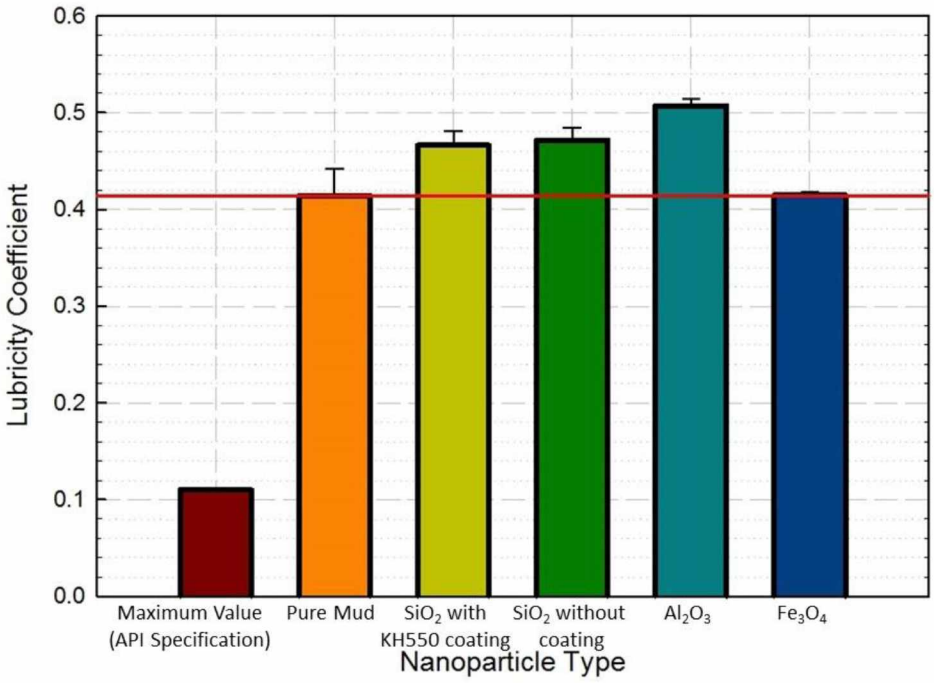

Figure 11: Effect of Nanoparticle Type on Lubricity Coefficient

4.2.4 Effect of Aging

In this scenario, the influence of aging on the lubricity of nanoparticle-based muds has been investigated. In this scenario, eight different nanoparticles, namely SiO_2 with KH550 coating, SiO_2 without coating, four different sizes of TiO_2 nanoparticles (5 nm, 10 nm, 15nm and 50 nm), Al_2O_3 and Fe_3O_4 have been tested at a concentration of 0.5 wt%, the results of which have been presented in Fig. 12.

Lubricity coefficient measurements for aged SiO_2 with KH550 and SiO_2 without coating nanoparticles were within relative standard deviation of 0.1% and 0.7%, respectively. While, aged different sizes of TiO_2 nanoparticle were within relative standard deviation of 2.5% for 5 nm, 0.6% for 10 nm, 0.3% for 15 nm and 0.2% for 50 nm. The relative standard deviations for Al_2O_3 and Fe_3O_4 nanoparticles were zero as the measurements were carried out only once, due to their limited amount. As can be seen in Fig. 12, aging has a significant effect on the lubricity coefficient of nanoparticle-based muds. In the case of the base mud, aging leads to an increase in the lubricity coefficient, which may be explained by dispersion of clay particles upon exposure to high temperatures. For both SiO_2 nanoparticles, aging decreases the lubricity coefficient, which may be due to the flocculation they cause, reducing the number of particles in suspension and improving the lubricity. However, the lubricity coefficient of the SiO_2 without coating nanoparticle is higher than that of the SiO_2 with KH550 coating nanoparticle due to a greater number of nanoparticles in dispersion. However, for TiO_2 nanoparticle, the trend for lubricity with increasing size remains moreover the same upon aging. In case of the TiO_2 5 nm nanoparticle, there might be breaking of agglomerated nanoparticles, leading to an increase in surface area and subsequent increase in friction. As explained in Section 4.1.4, upon aging, dissociation of clay might occur and due to presence of positive charge on TiO_2 nanoparticle particle aggregation can occur. Thus the combined effect of both the reasons may cause the lubricity coefficient trend observed for TiO_2 10 nm, TiO_2 15 nm, TiO_2 50 nm, Al_2O_3 and Fe_3O_4 nanoparticles. However, if we contrast the lubricity of nanoparticle-based muds with aged base mud (Fig. 12), aged SiO_2 with KH550 coating, SiO_2 without coating and Fe_3O_4 nanoparticles have lubricity coefficients lower than that of the aged base mud. This amounts to improvements of 4.81%, 2.93% and 9% for KH550 coating, SiO_2 without coating and Fe_3O_4 nanoparticles, respectively, compared to the aged base mud. Upon aging, these nanoparticles can improve the mud's lubricity compared to that of the aged base mud.

Also, lubricity coefficients for aged nanoparticle-based muds is greater than the maximum API value for lubricity coefficient. Therefore, aged nanoparticle-based muds do not satisfy the API lubricity requirement.

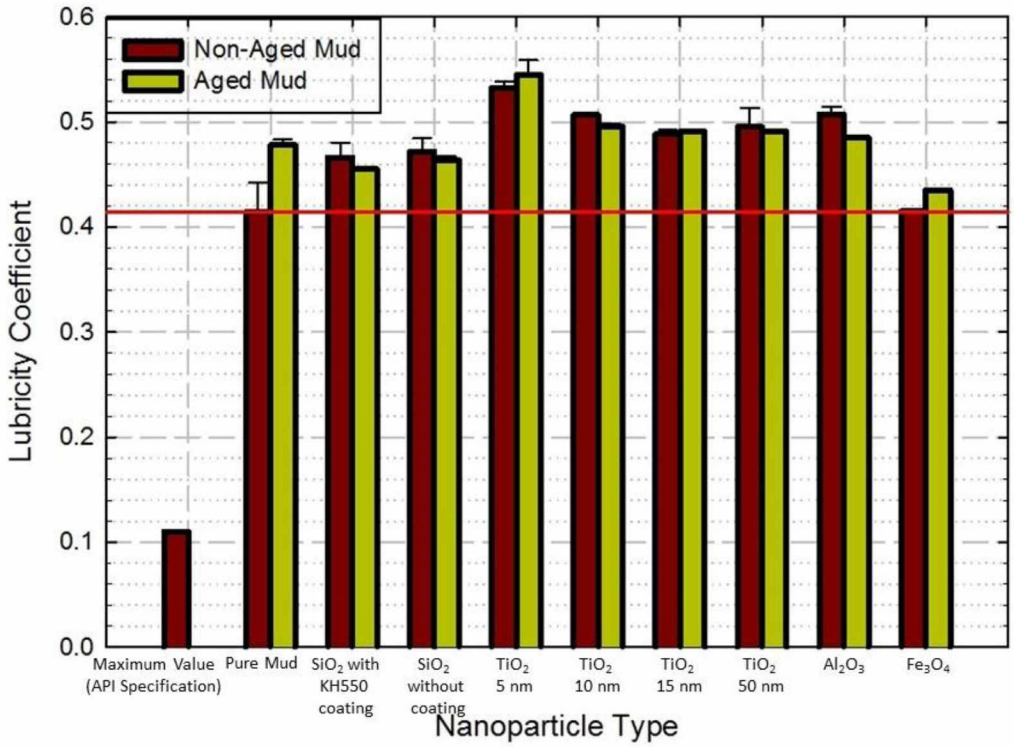

Figure 12: Effect of Aging on Lubricity Coefficient

4.3 The Influence on Filtration

In this subsection, the effects of nanoparticle concentration, nanoparticle size, nanoparticle type and aging on the filtration property of the nanoparticle-based muds have been investigated, while experimental results have been reported, analyzed and discussed. Also, the filtration loss of the nanoparticle-based muds has been compared to the API specification.

4.3.1 Effect of Concentration

In this scenario, the influence of nanoparticle concentration on the filtration property of nanoparticle-based muds has been investigated. Two nanoparticles, SiO_2 without coating and SiO_2 with KH550 coating, have been tested at concentrations of 0.01, 0.05, 0.1, 0.25, 0.5 and 1 wt%, the results of which have been presented in Fig. 13.

Filtration loss measurements for SiO_2 with KH550 nanoparticle were within an average relative standard deviation of 2.2%. While, SiO_2 without coating nanoparticle measurements were within 0.5%. Indicating, accuracy in measurements and good repeatability. As can be seen in Fig. 13, the filtration loss (FL) for both nanoparticles increases with increasing nanoparticle concentration. A potential reason for this behavior may be related to the propensity of nanoparticles to agglomerate. It may be that at low concentrations, the nanoparticles can effectively plug the pores due to a limited number of particles in dispersion, while at higher concentrations, they might start to agglomerate. The agglomerated nanoparticles form a highly porous/permeable layer beneath the main filter cake, thus increasing fluid loss (Mahmoud et al., 2016). In addition, greater filtration loss is observed for the SiO_2 without coating nanoparticle than the SiO_2 with KH550 coating nanoparticle. This may be due to the presence of a greater number of particles of the former than the latter nanoparticle. Also, it can be seen that FL for nanoparticle-based muds is lower than that of the base mud at lower concentration (< 0.25 wt%). Showing improvements of 11.9%, 9% and 10.9% for the SiO_2 with KH550 coating nanoparticle, and 6.25%, 4.38% and 1.9% for the SiO_2 without coating nanoparticle, at 0.01, 0.05 and 0.1 wt%, respectively. This indicates that, compared with the base mud, adding a small amount of SiO_2 nanoparticles (< 0.25 wt%) can improve the mud's filtration characteristics, while higher SiO_2 nanoparticle concentrations (> 0.25 wt%) have an adverse effect on filtration property of the mud. As the maximum value of FL in API specification is same as the FL in case of the base mud, it can stated that at low SiO_2 nanoparticle concentrations (< 0.25 wt%), the prepared nanoparticle-based muds satisfy the API requirement. While, at higher SiO_2 nanoparticle concentration (> 0.25 wt%), the prepared nanoparticle-based muds do not satisfy the API requirement.

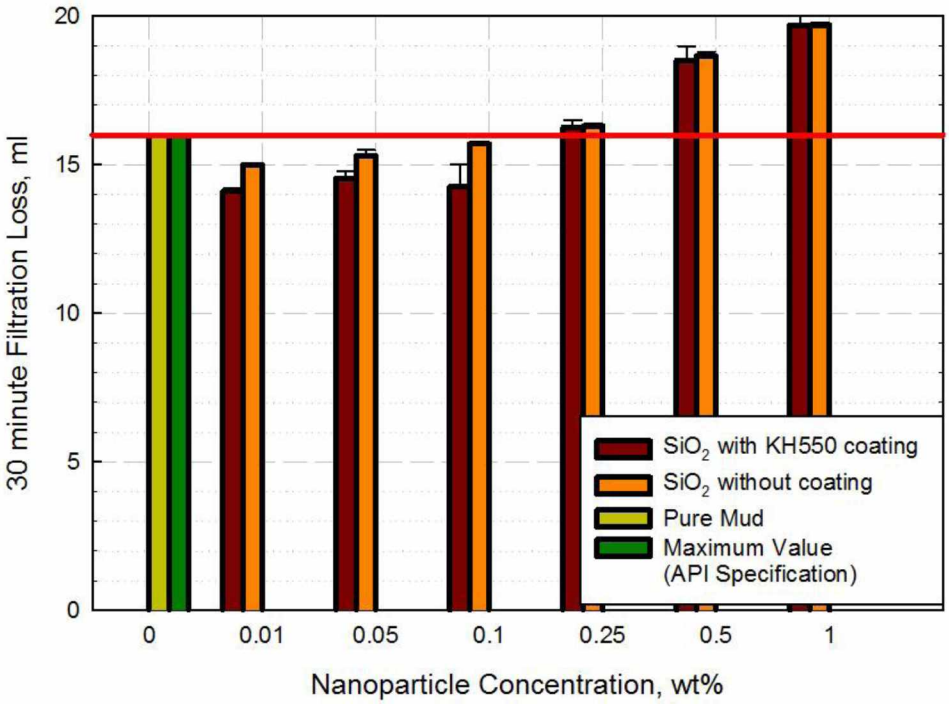

Figure 13: Effect of Nanoparticle Concentration on Filtration loss

4.3.2 Effect of Size

In this scenario, the influence of nanoparticle size on the filtration property of nanoparticle-based muds has been investigated. For this scenario, TiO_2 nanoparticles were tested at four different sizes, 5, 10, 15 and 50 nm, at a concentration of 0.5 wt%, the results of which have been presented in Fig. 14.

Filtration loss measurements for different sizes of TiO_2 nanoparticle were within relative standard deviation of 1.4% for 5 nm and 0.9% for 50 nm. While, the relative standard deviation for 10 nm and 15 nm was 0%. Indicating, good repeatability and precision of measurements. As can be seen in Fig. 14, filtration loss of nanoparticle-based muds decreases with increasing nanoparticle size from 5 nm to 10 nm, after which FL increases slightly with increasing size from 10 nm to 50 nm. The inability of the TiO_2 5 nm nanoparticle to limit FL may be due to its small size, because of which it might agglomerate more and form a porous/permeable nanoparticle layer beneath the filter cake, leading to increase in FL. Increases in size to 10 nm, 15 nm, and 50 nm have little effect on FL. For the 10 nm nanoparticle, FL is same as that of the base mud, while for nanoparticle sizes

of 15 nm and 50 nm, there is a minuscule increase in FL, which may be due to nanoparticle agglomeration. Therefore, in this scenario, the addition of different sizes of TiO_2 nanoparticle at 0.5 wt% does not improve the filtration characteristics of the mud. Also, the TiO_2 nanoparticle-based muds do not satisfy the API requirement at nanoparticle concentration of 0.5 wt%.

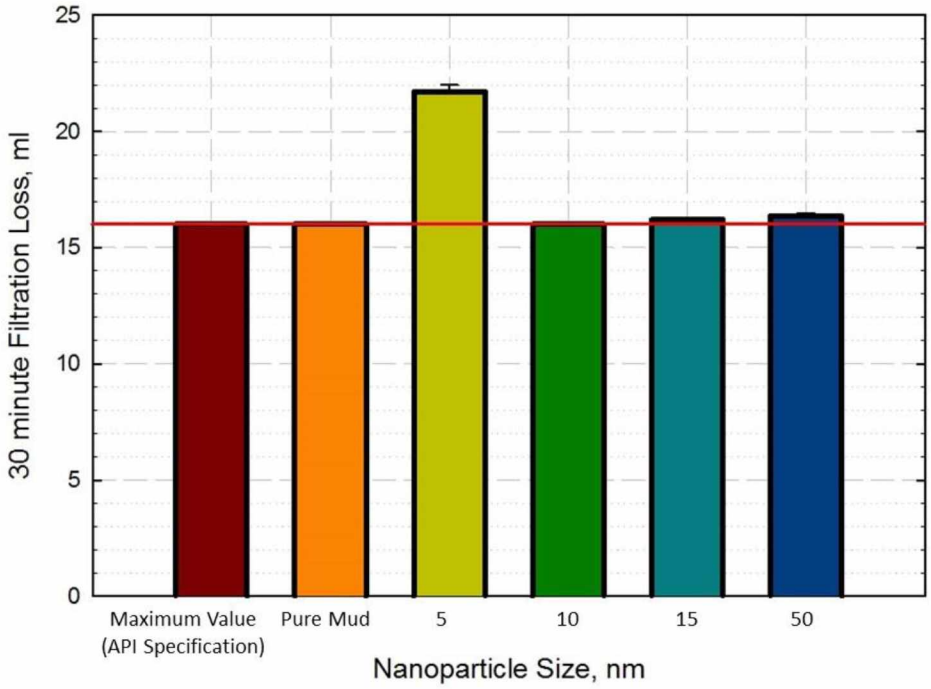

Figure 14: Effect of Nanoparticle Size on Filtration loss

4.3.3 Effect of Type

In this scenario, the influence of nanoparticle type on the filtration property of nanoparticle-based muds has been investigated. In this scenario, four different nanoparticles, namely Al_2O_3, Fe_3O_4 and two SiO_2 nanoparticles, one without any coating and other with KH550 coating, have been tested at a concentration of 0.5 wt%, the results of which have been presented in Fig. 15.

Lubricity coefficient measurements for SiO_2 with KH550, SiO_2 without coating, Al_2O_3 and Fe_3O_4 nanoparticles were within relative standard deviation of 2.7%, 0.8%, 4.2% and 1.9%, respectively. Indicating, good repeatability for all the tested nanoparticle types. As can be seen in Fig. 15, the filtration loss for nanoparticle-based muds is greater than for the base mud. The ascending order of increasing FL among the nanoparticles is Fe_3O_4, SiO_2 with KH550 coating, SiO_2 without

coating and Al_2O_3. The FL for both SiO_2 nanoparticles is comparable and, as discussed before, may be due to agglomeration of nanoparticles beneath the filter cake, which would not aid in effective plugging of pores and would lead to increased FL. FL is substantially greater for the Al_2O_3 nanoparticle, which might be due to its high degree of agglomeration caused in it, due to its large specific surface area, the number of particles and positive charge. Also, it forms a thicker mud cake, which would be permeable and quite porous, leading to greater FL. The FL for the Fe_3O_4 nanoparticle is slightly greater than that of the base mud and less than that of other nanoparticles, which may be due to its lesser number of particles in dispersion, pointing to slight nanoparticle agglomeration in the filter cake. Also, in this scenario, as the filtration loss of nanoparticle-based muds is greater than that of the base mud, the addition of different nanoparticles at a concentration of 0.5 wt% has an adverse effect on filtration characteristics of drilling mud. As the nanoparticle-based muds have filtration loss more than maximum filtration loss API value, they do not satisfy the API requirement.

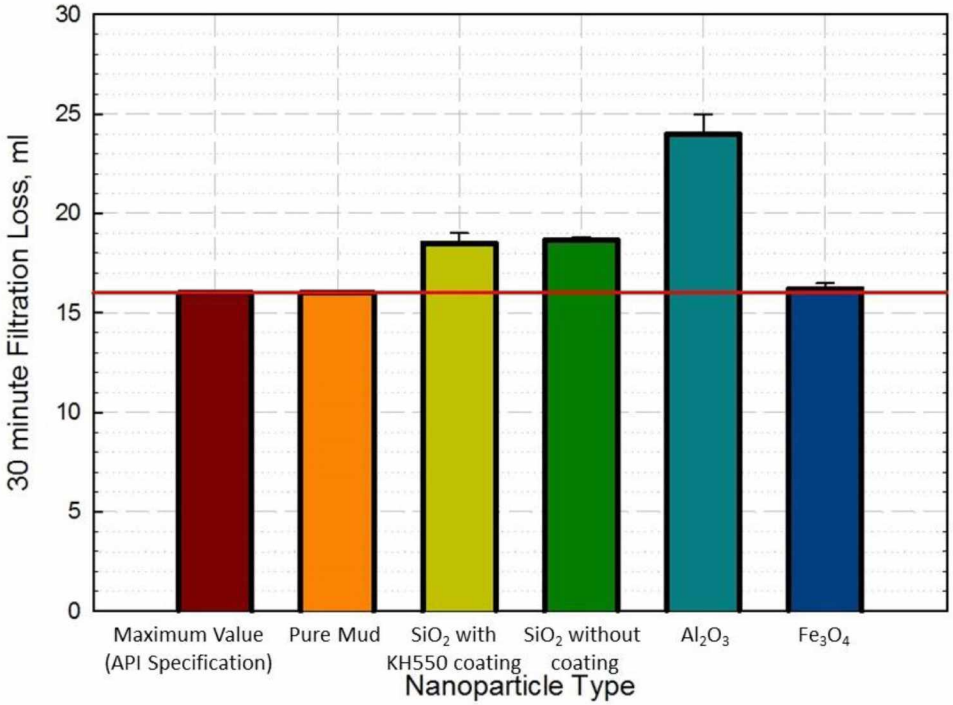

Figure 15: Effect of Nanoparticle Type on Filtration loss

4.3.4 Effect of Aging

In this scenario, the influence of aging on the filtration property of nanoparticle-based muds have been investigated. In this scenario, eight different nanoparticles, namely SiO_2 with KH550 coating, SiO_2 without coating, four different sizes of TiO_2 nanoparticles (5 nm, 10 nm, 15nm and 50 nm), Al_2O_3 and Fe_3O_4 have been tested at a concentration of 0.5 wt%, the results of which have been presented in Fig. 16.

Filtration loss measurements for aged SiO_2 with KH550 and SiO_2 without coating nanoparticles were within relative standard deviation of 2.9% and 0%, respectively. While, aged different sizes of TiO_2 nanoparticle were within relative standard deviation of 3.6% for 5 nm, 0% for 10 nm, 2.2% for 15 nm and 1.2% for 50 nm. The relative standard deviations for Al_2O_3 and Fe_3O_4 nanoparticles were zero as the measurements were carried out only once. As can be observed in Fig. 16, aging decreases filtration loss in nanoparticle-based muds. It is known that an increase in solid concentration of the mud increases the FL (Ismail et al., 1994). In the case of the base mud, aging leads to a slight increase in FL, which may be due to dissociation of clay particles upon exposure to high temperatures. For both SiO_2 nanoparticles, aging causes decrease in FL, which may be attributed to reduced agglomeration of nanoparticles in the filter cake. Similarly, the decrease in FL for TiO_2 5 nm, TiO_2 10 nm, TiO_2 15 nm, TiO_2 50 nm, Al_2O_3 and Fe_3O_4 nanoparticles after aging may be due to decrease in agglomeration of nanoparticles. Also, it can be seen that TiO_2 10 nm, TiO_2 15 nm and Fe_3O_4 nanoparticles have FL less than that of aged mud, showing improvements of 7.4%, 2.16% and 2.47%, respectively. This indicates that after aging, TiO_2 50 nm, Al_2O_3 and Fe_3O_4 nanoparticles can limit fluid loss better than aged base mud. While on comparison with the non-aged base mud, aged TiO_2 10 nm nanoparticle shows better filtration characteristics and satisfies the API requirement.

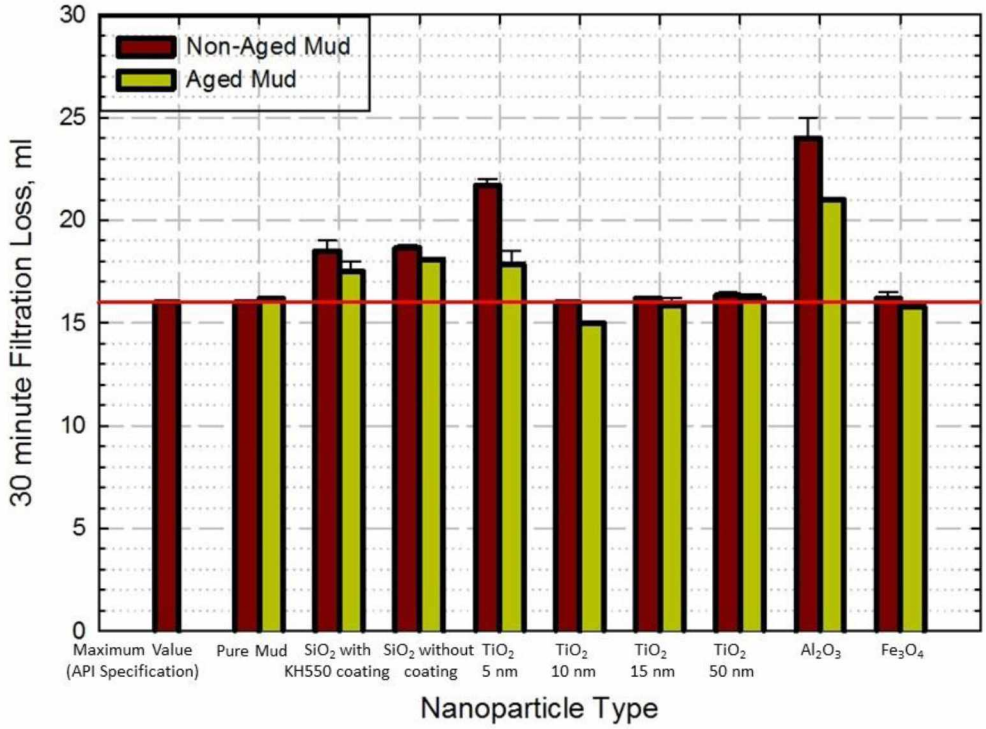

Figure 16: Effect of Aging on Filtration loss

Chapter 5.

CONCLUSIONS

This research investigated the influence of various nanoparticles on drilling fluid's rheological properties, lubricity and filtration characteristics. For clarity, the main points drawn from the experimental results are presented below.

1. Addition of negatively charged nanoparticles improved the hole cleaning function of the mud at low nanoparticle concentrations (<0.1 wt%).
2. Addition of positively charged nanoparticles improved the hole cleaning function of the mud.
3. Aging generally reduced the hole cleaning capability of the drilling fluids. Two nanoparticles, TiO_2 5 nm and Al_2O_3 nanoparticles, retained their hole cleaning capability after the aging process.
4. Increasing temperature, generally improves the hole cleaning capacity of the mud.
5. At low nanoparticle concentration (<0.1 wt%), lubricity for silica nanoparticle-based muds was improved. With, SiO_2 with KH550 coating nanoparticle performing better than SiO_2 without coating nanoparticle. While other tested nanoparticles failed to improve the lubricity of the mud.
6. Aging had a mixed effect on the mud's lubricity characteristics. For base mud, it decreased the lubricity, while for majority nanoparticle-based muds it slightly improved the lubricity.
7. At low nanoparticle concentration (<0.25 wt%), filtration characteristics of the silica nanoparticle-based muds were improved. At low nanoparticle concentration, the addition of SiO_2 with KH550 coating nanoparticle reduced filtration loss better than SiO2 without coating nanoparticle. Other nanoparticles failed to improve the filtration characteristics of the mud.
8. Upon aging, all the nanoparticle-based muds recorded decrease in fluid loss, with TiO_2 10 nm showing less fluid loss than base mud.

Chapter 6.

RECOMMENDATIONS

The primary objective of this study was to test the influence of nanoparticles on water-based mud. An experimental investigation of how nanoparticles affect mud properties was carried out by examining how mud's properties change with respect to nanoparticle concentration, size, type, aging and temperature. Even though the current study was thorough, it still has scope for extension and improvement in future. A few recommendations related to extending this work are presented below.

1. Unexpected results must be reinvestigated. For example, filtration characteristics for aged TiO_2 10 nm nanoparticle should be redetermined as, it was the only nanoparticle which recored less filtration loss compared to the base mud. Also, rhelogical properties of TiO_2 5 nm nanoparticle should redetermined as significant error was associated with them.
2. The effect of nanoparticles should be investigated on formation damage.
3. The effect of nanoparticle concentration on positively charged nanoparticles should be investigated.
4. For silica nanoparticles, the effect of nanoparticle concentration should be examined at nanoparticle concentrations lower than 0.01 wt%.
5. The colloidal stability of nanoparticle-based muds should be studied.
6. Scanning electron microscope (SEM) imaging and X-ray Defraction (XRD) analysis should be carried out for nanoparticle-based muds and their filter cakes, in order to understand the interaction of nanoparticles with the clay particles.
7. Different aging temperatures should be tested to study the effects of aging.
8. High temperature high pressure (HTHP) filtration on nanoparticle-based muds should be examined.

REFERENCES

Abdo, J.; and Haneef, M.D. Clay nanoparticles modified drilling fluids for drilling deep hydrocarbon wells. Applied Clay Science 2013, 86, 76-82.

Al-Yasiri, M.S.; and Al-Sallami, W.T. How the drilling fluids can be made more efficient by using nanomaterials. American Journal of Nano Research and Applications 2015, 3(3), 41-45.

API Specification 13A, 2011. Purchasing Guidelines Handbook. American Petroleum Institute, Washington, DC. USA.

API Recommended Practice 13B-1, 2009. Recommended Practice for Field Testing Water-Based Drilling Fluids. American Petroleum Institute, Washington, DC. USA.

API Recommended Practice 13BI, 2009. Recommended Practice for Standard Procedure for Laboratory Testing Water-Based Drilling Fluids. American Petroleum Institute, Washington, DC. USA.

Bloys, B.; Smolen, B.; Bailey, L.; Fraser, L.; and Holding, M. Designing and Managing Drilling Fluid. Oilfield Review 1994, 4, 33–43.

Bloodworth, B.R.; Keely, G.J.Jr.; and Clark, P.E. Mud relaxation measurements help predict hole cleaning ability. Oil and Gas Journal 1992, 90(22), 73-78.

Cai, J.; Chenevert, M.E.; Sharma, M.M.; and Friedheim, J. Decreasing water invasion into atoka shale using nonmodified silica nanoparticles. Paper SPE 146979 presented at the SPE Annual Technical Conference and Exhibition, Denver, Colorado, USA, 30 October-2 November, 2011.

Fakoya, M.F.; and Shah, S.N. Rheological properties of surfactant-based and polymeric nano-fluids. Paper SPE 163921 presented at SPE/ICoTA Coiled Tubing and Well Intervention and Exhibition, Woodlands, Texas, USA, 26-27 March, 2013.

Fakoya, M.F.; and Shah, S.N. Enhancement of filtration properties in surfactant-based and polymeric fluid by nanoparticles. Paper SPE 171029 presented at SPE Eastern Regional Meeting, Charleston, West Virgina, USA, 21-23 October, 2014.

Growcock, F.B.; and Patel, A.D. The Revolution in non-aqueous drilling fluids. Paper presented at the National Technical Conference and Exhibition, Houston, Texas, USA, 12-14 April, 2011.

Ismail, A.R.; Peden, J.M.; and Arshad, A.M. The effect of solids concentration and formation characteristics on formation damage and permeability recovery. Paper SPE 28762 presented at the SPE Asia Pacific Oil & Gas Conference, Melbourne, Australia, 7-10 November, 1994.

Jones, J.R. Lubrication, Friction, and Wear. NASA, Hampton, Virginia 23365, 1971.

Jung, Y.; Son, Y.H.; Lee, J.K.; Phuoc, T.X.; Soong, Y.; and Chyu, M.K. Rheological behavior of clay-nanoparticle hyprid-added bentonite suspensions: spcific role of hybrid additives on gelation of clay-based fluids. Applied Materials & Interfaces 2011, 3, 3515–3522.

Kang, Y.; She, J.; Zhang, H.; You, L.; and Song, M. Strengthening shale wellbore with silica nanoparticles drilling fluid. Petroleum 2016, 2(2), 189–195.

Kim, K.M.; Kim, H.M.; Lee, W.J.; Lee, C.W.; Kim, T.I.; Lee, J.K.; Jeong, J.; Paek, S.M.; and Oh, J.M. Surface treatment of silica nanoparticles for stable and charge controlled colloidal silica. International Journal of Nanomedicine 2014, 9(2), 29–40.

Li, Y.; Kroger, M.; and Liu, W.K. Nanoparticle geometrical effect on structure, dynamics and anisotropic viscosity of polyethylene nanocomposites. Macromolecules 2012, 45(4), 2099–2112.

Loosli, F.; Vitorazi, L.; Berret, J.F.; and Stoll, S. Towards a better understanding on agglomeration mechanisms and thermodynamic properties of TiO_2 nanoparticles interacting with natural organic matter. Water Research 2015, 80, 139–148.

Mahmoud, O.; Nasr-El-Din, H.A.; Vryzas, Z.; and Kelessidis, V.C. Nanoparticle-based drilling fluids for minimizing formation damage in HP/HT application. Paper SPE 178949 presented at the SPE International Conference and Exhibition on Formation Damage, Lafayette, Louisiana, USA, 24-26 February, 2016.

Mitchell, R.K.; Bethke, M.E.; and Dearing, H.L. Design and application of a high-temperature mud system for hostile environments. Paper SPE 20436 presented at the 65th SPE Annual Technical Conference and Exhibition, New Orleans, Louisiana, USA, 23-26 September, 1990.

MISWACO, 1998. *MISACO Drilling Fluid Manual*. MISWACO, USA.

Mondshine, T.C. A new potassium based mud system. Paper SPE 4516 presented at the 48th Annual Fall Meeting of Society of Petroleum Engineers of AIME, Las Vegas, Nevada, USA, 30 Sepetember-3 October, 1973.

Moslemizadeh, A.; and Shadizadeh, S.R. Minimizing water ivasion into kazhdumi shale using nanoparticles. Iranian Journal of Oil & Gas Science and Technology 2015, 4(4), 15–32.

Nasser, J.; Jesil, A.; Mohiuddin, T.; Rugeshi, M.; Devi, G.; and Mohataram, S. Experimental Investigation of Drilling Fluid Performance as Nanoparticles. World Journal of Nano Science and Engineering 2013, 3, 57–61.

Neff, J.M. *Fate and effects of water based drilling muds and cuttings in cold water environments*. Shell Exploration and Production Company, Houston, 2010.

Newhouse, C.C. Successfully drilling severely depleted sands. Paper SPE 21913 presented at the SPE/IADC Drilling Conference, Amsterdam, Netherlands, 11-14 March, 1991.

OFITE. *Model 900 Viscometer*. OFITE Testing Equipment, Inc., Houston, 2015.

OFITE. *API Filter Press*. OFITE Testing Equipment, Inc., Houston, 2013.

OFITE. *EP(Extreme Pressure) and Lubricity Tester*. OFITE Testing Equipment, Inc., Houston, 2015.

OFITE. *Portable Roller Oven*. OFITE Testing Equipment, Inc., Houston, 2015.

Okrajni, S.; and Azar, J.J. The effects of mud rheology on annular hole cleaning in direction wells. SPE Drilling Engineering 1986, 1(4), 297-308.

Patel, A.; Stamatakis, E.; Yong, S.; and Friedheim, J. Advances in inhibitive water-based drilling fluids – can they replace oil-based muds? Paper SPE 106476, presented at the International Symposium on Oilfield Chemistry, Houston, Texas, USA, 28 February-2 March, 2007.

Pham, H.; and Nguyen, Q.P. Effect of silica nanoparticles on clay swelling and aqueous stability of nanoparticle drispersions. Journal of Nanoparticle Research 2014, 16(1), 2137.

Ravi, A. Experimental assessment of water based drilling fluids in high pressure and high temperature conditions. Master's Thesis, Texas A&M University, College Station, Texas, USA, 2011.

Ravichandran, R. Nanotechnology Applications in Food and Food Processing: Innovative Green Approaches, Opportunities and Uncertainties for Global Market. International Journal of Green Nanotechnology: Physics and Chemistry 2010, 1, 72–96.

Redburn, M.; Dearing, H.; and Growcock, F. Field lubricity measurements correlate with improved performance of novel water-based drilling fluid. Paper, presented at the 11th Offshore Mediterranean Conference and Exhibition, Ravenna, Italy, 20-22 March, 2013.

Sami, N.A. Effect of magnesium salt contamination on the behavior of drilling fluids. Egyptian Journal of Petroleum 2015.

Salih, A.H.; Elshehabi, T.A.; and Bilgesu, H.I. Impact of nanomaterials on the rheological and filtration properties of water-based drilling fluids. Paper SPE 184067, presented at the SPE Eastern Regional Meeting, Canton, Ohio, USA, 13-15 September, 2016.

Sensoy, T.; Chenevert, M.E.; and Sharma, M.M. Minimizing water invasion in shale using nanoparticles. Paper SPE 124429 presented at SPE Annual Technical Conference and Exhibition, New Orleans, Louisiana, USA, 4-7 October, 2009.

Shah, S.N.; Shanker, N.H.; and Ogugbue, C.C. Future challenges of drilling fluids and their rheological measurements. Paper AADE-10-DF-HO-41 presented at AADE Fluids Conference and Exhibition, Houston, Texas, USA, 6-7 April, 2010.

Sharma, M.M..; Zhang, R.; Chenevert, M.E.; Ji, L.; Guo, Q.; and Friedheim, J. A new family of nanoparticle based drilling fluids. Paper SPE 160045 presented at SPE Annual Technical Conference and Exhibition, San Antonio, Texas, USA, 8-10 October, 2012.

Underbalanced drilling - Petrowiki. (n.d.). Retrieved from https://petrowiki.org/PEH%3AUnderbalanced_Drilling

Van Oort, On the physical and chemical stability of shales. Journal of Petroleum Science and Engineering, 38(3-4), 213-235.

Vryzas, Z.; Mahmoud, O.; Nasr-El-Din, H.A.; and Kelessidis, V.C. Development and testing of novel drilling fluids using Fe_2O_3 and SiO_2 nanoparticles for enhanced drilling operations. Paper IPTC 18381 presented at International Petroleum Technology Conference, Doha, Qatar, 6-9 December, 2015.

Wrobel, S. Development of an improved nanoparticle-modified water based drilling fluid. Master's Thesis, University of Stavanger, Stavanger, Norway, 2016.

Zakaria, M.F.; Husein, M.; and Hareland, G. Novel nanoparticle-based drilling fluid reveals improved characteristics. Journal of Petroleum Technology 2012, 11, 100–102.

APPENDIX

Table A-1: API Specifications for Bentonite (API Specification 13A)

Suspension Properties	Standard
Plastic Viscosity, cP	Minimum 7
Yield Point, D.R.	Maximum 46.95
YP/PV	Maximum 6
Lubricity Coefficient	Maximum 0.11
Filtrate Volume, ml	Maximum 16

Table A-2: Rheology Data for SiO_2 with KH550 coating

	Pure Mud	SiO_2 with KH550 coating					
Concentration, wt%	0	0.01	0.05	0.1	0.25	0.5	1
PV, cP	6.4825	6.879	7.653	8.604	8.792	9.7355	12.4705
YP, dial reading	8.844	14.506	12.1825	9.6285	5.4295	3.54	3.2025
n	0.1217	0.1007	0.11335	0.16555	0.2835	0.35295	0.46415
K	6.39625	10.58605	8.79705	5.69765	2.25425	1.21105	0.73925
Gel1	7.5	10	9	4.5	2	0.5	1
Gel2	13	18	15.5	13	8.5	6	6
YP/PV	1.364	2.109	1.592	1.119	0.618	0.364	0.257

Table A-3: Rheology Data for SiO_2 without coating

	Pure Mud	SiO_2 without coating					
Concentration, wt%	0	0.01	0.05	0.1	0.25	0.5	1
PV, cP	6.4825	7.0405	7.201	7.2235	9.698	11.849	12.8675
YP, dial reading	8.844	13.3045	12.1755	10.304	6.206	3.0655	2.6635
n	0.1217	0.09265	0.10215	0.13265	0.2717	0.514	0.52765
K	6.39625	10.18025	9.2059	6.81765	2.7405	0.58165	0.54925
Gel1	7.5	9	8.5	6	3	0.5	0.5
Gel2	13	17	16	13	9.5	5.5	5.5
YP/PV	1.364	1.890	1.691	1.426	0.640	0.259	0.207

Table A-4: Rheology Data for Different size of TiO_2

	Pure Mud	TiO_2 at 0.5 wt%			
Particle Size, nm	-	5	10	15	50
PV, cP	6.4825	8.0265	6.7975	6.075	5.587
YP, dial reading	8.844	31.7225	17.2135	19.942	20.005
n	0.1217	0.0839	0.089	0.07065	0.07185
K	6.39625	22.5927	12.94205	15.6166	15.6345
Gel1	7.5	29	14	16	16
Gel2	13	35	19.5	21.5	21.5
YP/PV	1.364	3.925	2.524	3.285	3.6

Table A-5: Rheology Data for Different Nanoparticle Types

	Pure Mud	SiO_2 with KH550 coating	SiO_2 without coating	Al_2O_3	Fe_3O_4
PV, cP	6.4825	9.7355	11.849	23.233	5.8295
YP, dial reading	8.844	3.54	3.0655	67.626	19.753
n	0.1217	0.35295	0.514	0.0768	0.07165
K	6.39625	1.21105	0.58165	42.302	15.565
Gel1	7.5	0.5	0.5	68	16
Gel2	13	6	5.5	75	22
YP/PV	1.364	0.364	0.259	2.91	3.39

Table A-6: Rheology Data for Aged Pure Mud and Silica

Tested Media	Pure Mud	SiO_2 with KH550 Coating	SiO_2 without coating
PV, cP	13.3625	17.78	18.902
YP, dial reading	7.3445	5.9715	5.9685
n	0.25685	0.3888	0.42295
K	3.4518	1.7745	1.5161
Gel1	3.5	2	2
Gel2	10.5	11.5	12.5
YP/PV	0.549	0.336	0.316

Table A-7: Rheology Data for Aged Different Sizes of TiO_2

Tested Media	TiO_2			
Particle Size, nm	5	10	15	50
PV, cP	6.79	11.051	13.548	15.602
YP, dial reading	21.9035	13.769	13.5945	14.901
n	0.07555	0.1408	0.16715	0.16515
K	17.00545	9.0227	8.31545	9.3129
Gel1	19.5	9.5	9	10.5
Gel2	27	16.5	16.5	19
YP/PV	3.292	1.253	1.007	0.955

Table A-8: Rheology Data for Aged Al_2O_3 and Fe_3O_4

Tested Media	Al_2O_3	Fe_3O_4
PV, cP	18.662	12.361
YP, dial reading	41.271	14.935
n	0.1069	0.1432
K	35.7772	9.7993
Gel1	62	10
Gel2	65	18
YP/PV	2.211	1.208

Table A-9: Rheology Data for Pure Mud

Pure Mud				
Temperature, °C	25	40	60	80
PV, cP	6.4825	3.702	3.123	1.616
YP, dial reading	8.844	12.141	15.076	16.373
n	0.1217	0.0736	0.068	0.0591
K	6.39625	9.5304	11.5085	12.5529
Gel1	7.5	10	13	15
Gel2	13	16	20	28
YP/PV	1.364	2.484	4.238	6.982

Table A-10: Rheology Data for SiO_2 with KH550 coating

SiO_2 with KH550 coating				
Temperature, °C	25	40	60	80
PV, cP	9.736	6.597	5.235	4.706
YP, dial reading	3.540	4.329	5.628	9.962
n	0.353	0.2463	0.1589	0.0872
K	1.211	1.9965	3.4987	7.8109
Gel1	0.500	2	3	7
Gel2	6.000	8	13	30
YP/PV	0.364	0.557	0.899	1.425

Table A-11: Rheology Data for SiO_2 without coating

SiO_2 without coating				
Temperature, °C	25	40	60	80
PV, cP	11.849	7.98	7.703	7.052
YP, dial reading	3.066	3.446	4.009	6.142
n	0.514	0.3313	0.2363	0.16
K	0.582	1.1972	2.2263	4.1337
Gel1	0.500	1	1	6
Gel2	5.500	8	11	24
YP/PV	0.259	0.765	1.056	1.447

Table A-12: Lubricity Coefficient for SiO_2 with KH550 coating

	Pure Mud	SiO_2 with KH550 coating					
Concentration, wt%	0	0.01	0.05	0.1	0.25	0.5	1
Lubricity Coefficient	0.414	0.374	0.389	0.436	0.458	0.466	0.470

Table A-13: Lubricity Coefficient for SiO_2 without coating

	Pure Mud	SiO_2 without coating					
Concentration, wt%	0	0.01	0.05	0.1	0.25	0.5	1
Lubricity Coefficient	0.414	0.394	0.407	0.471	0.470	0.472	0.478

Table A-14: Lubricity Coefficient for Different sizes of TiO_2

	Pure Mud	TiO_2 at 0.5 wt%			
Particle Size, nm	-	5	10	15	50
Lubricity Coefficient	0.414	0.532	0.507	0.488	0.495

Table A-15: Lubricity Coefficient for Different Nanoparticle Types

	Pure Mud	SiO_2 with KH550 coating	SiO_2 without coating	Al_2O_3	Fe_3O_4
Lubricity Coefficient	0.414	0.466	0.472	0.507	0.415

Table A-16: Lubricity Coefficient for Aged Pure Mud and Silica

Tested Media	Pure Mud	SiO2 with KH550 Coating	SiO2 without coating
Lubricity Coefficient	0.478	0.455	0.464

Table A-17: Lubricity Coefficient for Aged Different sizes of TiO_2

Tested Media	TiO_2			
Particle Size, nm	5	10	15	50
Lubricity Coefficient	0.545	0.496	0.491	0.491

Table A-18: Lubricity Coefficient for Aged Al_2O_3 and Fe_3O_4

Tested Media	Al_2O_3	Fe_3O_4
Lubricity Coefficient	0.485	0.435

Table A-19: Filtration Characteristics for SiO_2 with KH550 coating

	Pure Mud	SiO_2 with KH550 coating					
Concentration, wt%	0	0.01	0.05	0.1	0.25	0.5	1
30 minutes, ml	16	14.1	14.55	14.25	16.25	18.5	19.7
Mud Cake Thickness, in	0.125	0.125	0.125	0.125	0.125	0.09375	0.09375

Table A-20: Filtration Characteristics for SiO_2 without coating

	Pure Mud	SiO_2 without coating					
Concentration, wt%	0	0.01	0.05	0.1	0.25	0.5	1
30 minutes, ml	16	15	15.3	15.7	16.3	18.65	19.7
Mud Cake Thickness, in	0.125	0.125	0.125	0.125	0.125	0.125	0.125

Table A-21: Filtration Characteristics for Different Sizes of TiO_2

	Pure Mud	TiO2 at 0.5 wt%			
Particle Size, nm	-	5	10	15	50
30 minutes, ml	0.414	21.7	16	16.2	16.35
Mud Cake Thickness, in	0.125	0.1875	0.15625	0.125	0.125

Table A-22: Filtration Characteristics for Different Nanoparticle Types

	Pure Mud	SiO_2 with KH550 coating	SiO_2 without coating	Al_2O_3	Fe_3O_4
30 minutes, ml	16	18.5	18.65	24	16.2
Mud Cake Thickness, in	0.125	0.09375	0.125	0.28125	0.125

Table A-23: Filtration Characteristics for Aged Pure Mud and Silica

Tested Media	Pure Mud	SiO_2 with KH550 Coating	SiO_2 without coating
30 minutes, ml	16.2	17.5	18.1
Mud Cake Thickness, in	0.125	0.125	0.094

Table A-24: Filtration Characteristics for Aged Different sizes of TiO_2

Tested Media	TiO_2			
Particle Size, nm	5	10	15	50
30 minutes, ml	17.85	15	15.85	16.2
Mud Cake Thickness, in	0.125	0.125	0.125	0.125

Table A-25: Filtration Characteristics for Aged Al_2O_3 and Fe_3O_4

Tested Media	Al_2O_3	Fe_3O_4
30 minutes, ml	17.85	15
Mud Cake Thickness, in	21	15.8